On the Role of the Antarctic Slope Front on the Occurrence of the Weddell Sea Polynya under Climate Change

Joseph W. Lockwood,[a] Carolina O. Dufour,[a] Stephen M. Griffies,[b,c] and Michael Winton[b]

[a] *Department of Atmospheric and Oceanic Science, McGill University, Montreal, Quebec, Canada*
[b] *National Oceanic and Atmospheric Administration, Geophysical Fluid Dynamics Laboratory, Princeton, New Jersey*
[c] *Atmospheric and Oceanic Sciences Program, Princeton University, Princeton, New Jersey*

ABSTRACT: This study investigates the occurrence of the Weddell Sea polynya under an idealized climate change scenario by evaluating simulations from climate models of different ocean resolutions. The GFDL-CM2.6 climate model, with roughly 3.8-km horizontal ocean grid spacing in the high latitudes, forms a Weddell Sea polynya at similar time and duration under idealized climate change forcing as under preindustrial forcing. In contrast, all convective models forming phase 5 of the Coupled Model Intercomparison Project (CMIP5) show either a cessation or a slowdown of Weddell Sea polynya events under climate warming. The representation of the Antarctic Slope Current and related Antarctic Slope Front is found to be key in explaining the differences between the two categories of models, with these features being more realistic in CM2.6 than in CMIP5. In CM2.6, the freshwater input driven by sea ice melt and enhanced runoff found under climate warming largely remains on the shelf region since the slope front restricts the lateral spread of the freshwater. In contrast, for most CMIP5 models, open-ocean stratification is enhanced by freshening since the absence of a slope front allows coastal freshwater anomalies to spread into the open ocean. This enhanced freshening contributes to the slowdown the occurrence of Weddell Sea polynyas. Hence, an improved representation of Weddell Sea shelf processes in current climate models is desirable to increase our ability to predict the fate of the Weddell Sea polynyas under climate change.

KEYWORDS: Sea ice; Southern Ocean; Boundary currents; Deep convection; Climate models

1. Introduction

Over the winters of 1974–76, satellite observations from the *Nimbus-5* Electrically Scanning Microwave Radiometer revealed the presence of a large polynya within the Antarctic pack ice of the Weddell Sea (Carsey 1980), covering an estimated time average area of $250 \times 10^3 \, \text{km}^2$ (Gordon et al. 2007). This polynya, known as the Weddell Sea polynya, was maintained by intense vertical convection of warm water from depth (Martinson et al. 1981). The heat responsible for the formation of the polynya was advected from a subsurface heat reservoir located in the Weddell Deep Water in the Weddell Sea. The subsurface heat reservoir is identified by a water column temperature maximum between 0° and 1.3°C in the depth range of approximately 130 to 1600 m (Smedsrud 2005). During convection, this warm water was directly exposed to the atmosphere. This process induced a buoyancy exchange such that the newly exposed water cooled, releasing heat to the atmosphere, before subsequently sinking back to the deep ocean and forming intense chimneys of convection extending down to 3000 m (Gordon 1978). The upward flux of heat during convection and subsequent cooling at depth are thought to have

contributed to the formation of the Antarctic Bottom Water for the following decade, thus acting to intensify global ocean overturning circulation (Gordon 1978). Observational estimates from Gordon (1982) suggest that the volume flux of surface water injected into depth during the Weddell Sea polynya was between 1.6 and 3.2 Sv (1 Sv = $10^6 \, \text{m}^3 \, \text{s}^{-1}$). In addition, reconstructions of the air–sea interaction associated with this polynya suggest large localized atmospheric perturbations with ocean-to-atmosphere moisture and heat losses causing +20°C surface (2 m) air temperature anomalies and 50% higher cloud cover over the polynya during several months of 1976 compared to climatology (Moore et al. 2002).

Since the initial observation of the Weddell Sea polynya in the 1970s, a number of mechanisms have been proposed to overcome the regionally weak salinity stratification, thus initiating the convection events. These mechanisms include intense surface cooling and brine rejection during sea ice formation (Martinson et al. 1981), enhanced horizontal cyclonic oceanic eddy activity (Holland 2001), and Taylor column circulation (Kurtakoti et al. 2018) at the Maud Rise. A transition of the southern annular mode from a prolonged negative phase to a positive phase may have also contributed to the formation of the Weddell Sea polynya, with negative phases resulting in high surface salinity anomalies due to drier and colder surface conditions (Gordon et al. 2007) and positive phases resulting in a strengthening of the Southern Hemisphere westerlies, the combination of which initiates convection (Cheon et al. 2014). Once initiated, deep convection will have continued until either the depletion of the subsurface heat reservoir (Martin et al. 2013) or input of

---

freshwater to the surface (Comiso and Gordon 1987), both of which will have re-established water column stability.

The occurrence of a similar polynya in the Weddell Sea region was not observed again until the winters of 2016 and 2017, when a large sea ice hole opened over the Maud Rise (Campbell et al. 2019; Jena et al. 2019). Despite being the largest polynya observed at the Maud Rise since 1980 (Cheon and Gordon 2019), these polynyas were substantially smaller compared to the 1970s Weddell Sea polynya, stabilizing at approximately $50 \times 10^3 \, \mathrm{km}^2$ (~20% of the 1970s polynya) between September and November 2017 (Jena et al. 2019). Unlike the 1970s polynya, which propagated westward from the Maud Rise into the open ocean at an average velocity of $0.013 \, \mathrm{m \, s}^{-1}$ (Gordon 1978, 1982), this recent event remained at the Maud Rise. Analyses of observations over the winters of 2016 and 2017 have suggested that this event was preconditioned by wind-driven upwelling that weakened the haline stratification (Campbell et al. 2019; Cheon and Gordon 2019). The initiation of these events has been linked to the passage of severe cyclones causing sea ice divergence and turbulent mixing (Campbell et al. 2019; Francis et al. 2019). Enhanced poleward meridional transport of heat and moisture, associated with an amplification of the atmospheric zonal wave 3 and a strong positive southern annular mode index, may have contributed to polynya formation over these winters (Francis et al. 2019). Wind-induced spinup of the cyclonic Weddell Gyre and strong negative wind curl over the Maud Rise are also suggested to have led to the formation of the 2017 polynya (Cheon and Gordon 2019).

Among the models from phase 5 of the Coupled Model Intercomparison Project (CMIP5) models, deep ocean convection is common in the Southern Ocean under preindustrial simulations (de Lavergne et al. 2014), although these events are often categorized as spurious as most models overestimate spatial extent compared to observations (Heuzé et al. 2013). Antarctic Bottom Water formation in CMIP5 models is primarily controlled by these convection events, as coastal processes leading to the formation and cascading of dense shelf waters down the continental slope are not resolved in these relatively coarse-resolution models. CMIP5 models, therefore, often exhibit biases in Southern Ocean water mass properties and stratification (Heywood et al. 2014), as well as in their representation of large-scale ocean dynamics such as the Antarctic Circumpolar Current (Beadling et al. 2019).

Recent studies utilizing models with relatively fine ocean horizontal grid spacing (≤1 km) have allowed for the investigation of finer-scale processes in the Southern Ocean. These models have revealed that mesoscale eddies support a significant transport of heat and mass across the Antarctic Slope Front (Stewart and Thompson 2015), a front observed in most regions of Antarctica that presents a strong barrier to tracer transport (Thompson et al. 2018). The inability of CMIP5 models to capture the dynamics on the shelf and fine-scale processes in that region may result in biases in the mean state circulation and water mass properties, in turn impacting climate change projections. Notably, under climate change simulations, open-ocean convection in CMIP5 models has been reported to slow down, and associated polynyas to occur less frequently or even cease, owing to enhanced upper ocean stratification (de Lavergne et al. 2014). In contrast, our analysis of the Geophysical Fluid Dynamics Laboratory (GFDL) CM2.6 global climate model, with an ocean component of 0.1° horizontal grid spacing (~3.8 km at 70°S) reveals a continuation of convection events and of the Weddell Sea polynya under a climate change simulation (section 3). Considering the atmospheric and oceanic changes brought about by polynya formation, an accurate representation of convection and polynya formation in the Southern Ocean is required to ensure reliable model projections of regional and global climate. Understanding the physical mechanisms accounting for the different behavior found in CM2.6 versus CMIP5 is the goal of this paper.

Our hypothesis is that, because of their relatively coarse ocean resolutions, the CMIP5 models are unable to represent important processes involved in the formation of polynyas and in their response to climate change. To investigate this hypothesis, we use preindustrial control (piControl) and idealized 1% yr^{-1} carbon dioxide (CO_2) rise (1pctCO$_2$) simulations of CM2.6 and of CMIP5 models to investigate the response of the Weddell Sea polynya to climate change (section 2). We first compare the occurrence of open-ocean deep convection and Weddell Sea polynya events in the models under the piControl and 1pctCO$_2$ simulations (section 3). We find a strong relationship between convection events, surface salinity, and vertical density stratification under climate change (section 4), and a freshening at the surface which is driven by enhanced runoff and sea ice change (section 5). In CM2.6, the spatial distribution of freshening is predominantly confined to the coasts due to the barrier provided by the Antarctic Slope Current (ASC) and Antarctic Slope Front (ASF; section 6). In section 7a, we evaluate the ability of CM2.6 and CMIP5 models to represent the ASF and ASC by comparing them to the ultrafine resolution LLC_4320 model (1/48° horizontal grid spacing; Rocha et al. 2016). Although CM2.6 lacks certain of the fine-scale features found in LLC_4320, this model–model comparison shows that CM2.6 provides a more realistic representation of the ASF and ASC than CMIP5 models. In section 7b we discuss the relation between ASC strength and open-ocean freshening and in section 7c the conditions for reoccurrence of the Weddell Sea polynya in the future.

2. Methods

a. Models

1) THE GFDL CM2.6 CLIMATE MODEL

The GFDL CM2.6 climate model, which is part of the GFDL CM2-O climate model suite, is the key tool for this study (Delworth et al. 2012; Griffies et al. 2015). CM2.6 has a horizontal atmospheric grid spacing of 0.45° with 32 vertical levels formulated on a cubed-sphere grid, in which the atmosphere is represented on the six sides of a cube. CM2.6's ocean component uses version 5 of the Modular Ocean Model (MOM5; Griffies et al. 2015) with volume-conserving Boussinesq kinematics. The horizontal grid is tripolar, with two poles in the

TABLE 1. List of the models used with their respective ocean and atmospheric horizontal resolutions, and treatment of gravitational instability in the ocean.

Model	Ocean resolution	Atmosphere resolution	Gravitational instability
CM2.6	0.1°	0.45°	Enhanced vertical diffusivity and viscosity
ACCESS1.0	1°	1.25° × 1.875°	Enhanced vertical diffusion
ACCESS1.3	1°	1.25° × 1.875°	Enhanced vertical diffusion
BCC-CSM1.1	0.33°–1°	2.7° × 2.8°	Enhanced vertical diffusion
BCC-CSM1.1m	0.33°–1°	2.7° × 2.8°	Enhanced vertical diffusion
CNRM-CM5	1° × 0.65°	1.4°	Enhanced vertical diffusion
CNRM-CM5.2	1° × 0.65°	1.4°	Enhanced vertical diffusion
CSIRO-Mk3.6.0	1.8° × 0.93°	1.8°	Convective adjustment
CSIRO-Mk3L-1.2	2.8° × 1.6°	3.2° × 5.6°	Enhanced vertical diffusion
FGOALS-g2	0.5°–1°	2.8°	Convective adjustment
FGOALS-s2	0.5°–1°	1.6° × 2.8°	Convective adjustment
GFDL CM3	0.33°–1°	2° × 2.5°	Enhanced vertical diffusion
GFDL-ESM2G	0.33°–1°	2°	Included turbulence closure
GFDL-ESM2M	0.33°–1°	2° × 2.5°	Enhanced vertical diffusion
HadGEM2-ES	0.33°–1°	1.25° × 1.8°	Enhanced vertical diffusion
INM-CM4	0.5°–1°	1.5° × 2°	Enhanced vertical diffusion
IPSL-CM5A-LR	1.9° × 1.3°	1.8° × 3.75°	Enhanced vertical diffusion
IPSL-CM5A-MR	1.9° × 1.3°	1.2° × 2.5°	Enhanced vertical diffusion
IPSL-CM5B-LR	1.9° × 1.3°	1.8° × 3.75°	Enhanced vertical diffusion
MIROC5	0.5° × 1.4°	1.4°	Convective adjustment
MPI-ESM-LR	1.5°	1.8°	Enhanced vertical diffusion
MPI-ESM-MR	0.4°	1.8°	Enhanced vertical diffusion
MPI-ESM-P	1.4° × 1°	1.8°	Enhanced vertical diffusion
MRI-CGCM3	0.5° × 1°	1°	Convective adjustment

Northern Hemisphere and one at the South Pole (Murray 1996). The vertical grid has 50 levels with thicknesses of 10 m at the surface increasing with depth to 210 m. CM2.6 has a horizontal ocean grid spacing of 0.10°, corresponding to a grid size of 3.8 km at 70°S. CM2.6 is an eddy-rich model at midlatitudes, notably in the Antarctic Circumpolar Current (Delworth et al. 2012; Griffies et al. 2015), and therefore does not employ a mesoscale eddy parameterization. However, CM2.6 does not fully resolve mesoscale eddies on high-latitude continental shelves, which requires roughly a 1-km horizontal resolution (St-Laurent et al. 2013; Hallberg 2013). Sea ice is simulated by the GFDL Sea Ice Simulator (SIS), which is a dynamical model with three vertical layers, one snow and two ice, and five ice-thickness categories (Winton 2000). The sea ice model uses the same horizontal tripolar grid as the ocean component.

Vertical mixing in CM2.6 is determined by the *K*-profile parameterization (KPP) scheme (Large et al. 1994). Within this boundary layer, the turbulent mixing is parameterized using a nonlocal bulk Richardson number. Below the boundary layer, vertical mixing is parameterized through the local gradient Richardson number. The Fox-Kemper et al. (2011) parameterization is employed to represent submesoscale mixed layer eddies. Regions of gravitational instability are stabilized by enhanced vertical diffusivity and viscosity (Klinger et al. 1996). A description of the representation of the Southern Ocean and Antarctic coasts in CM2.6 can be found in Griffies et al. (2015) [see also Dufour et al. (2017) and Goddard et al. (2017)]. For the 1pctCO$_2$ experiment, note that CM2.6 has

a relatively high transient climate response of 2 K (Winton et al. 2014).

2) CMIP5 MODELS

CMIP5 models comprise a range of climate models and Earth system models, differing from each other in terms of model structure, including vertical coordinate, grid resolution, and subgrid parameterizations (Taylor et al. 2012). We analyzed all CMIP5 models for which the following monthly output were available for the investigated experiments (see section 2b): sea ice concentration (sic), potential temperature (thetao), and salinity (so). The resulting 23 CMIP5 models used in this study have horizontal ocean grid spacing generally ≥1°. Due to their relatively coarse ocean resolution, the transport and mixing by mesoscale eddies are parameterized in the CMIP5 models. Some processes representative of surface waves and tides are taken into account in the parameterization of vertical mixing in a number of CMIP5 models used. The full list of models used in this study, along with horizontal grid spacings and treatment of oceanic gravitational instabilities, is available in Table 1. Note that "CMIP5 model means" correspond to all 23 CMIP5 models, unless otherwise stated. Although all analyses were performed on all models with output available, in the following we highlight four convective models of varying horizontal ocean resolution (from 1° to 0.4°)—ACCESS1.0, GFDL CM3, MPI-ESM-LR, and MPI-ESM-MR—and one nonconvective model with a horizontal ocean resolution of 1°, HadGEM2-ES (Table 1). The

multimodel mean transient climate response for the full suite of atmosphere–ocean general circulation CMIP5 models is 1.8 K over the 1pctCO$_2$ experiment (Flato et al. 2013). CMIP5 models are therefore generally less sensitive to the 1pctCO$_2$ experiment compared to CM2.6.

3) LLC_4320 MODEL

LLC_4320 is an ocean–sea ice model based on the MIT general circulation model (MITgcm; Rocha et al. 2016), configured with the very fine horizontal grid spacing of 1/48°. It also has 90 depth levels, ranging from 1 m at the surface to 480 m at a depth of 7000 m. The 16 most dominant astronomical tidal forcing components are included to allow for the representation of realistic tides. In addition, the simulation is forced by 6-hourly 0.14°European Centre for Medium-Range Weather Forecasts analysis (ECMWF 2011).

With its very fine grid spacing, the LLC_4320 simulation resolves mesoscale eddies on the continental shelves of Antarctica and is the first ocean–sea ice model capable of resolving circum-Antarctic mean flows, eddies, and tides together (Stewart et al. 2018). The bathymetry of LLC_4320 differs from that of the real ocean, and the model underestimates Dense Shelf Water (DSW) on the Antarctic Shelf (Stewart et al. 2019). Despite these caveats, the LLC_4320 shows good congruence to observations and produces a realistic ASF (Stewart et al. 2019). With its ultrafine resolution, LLC_4320 is primarily used here to discuss the effect of resolution on the representation of the ASC/ASF. Furthermore, it is used to evaluate the resolutions of CM2.6 and CMIP5 models at the shelf break as it allows for comparison in all seasons and under sea ice, in contrast to observations.

The LLC_4320 output we use is described in Stewart et al. (2018) and spans September 2011 to October 2012, where 6-h snapshots are averaged over the full time period. The model output was retrieved from a publicly available repository (http://metadata.imas.utas.edu.au/geonetwork/srv/eng/metadata.show?uuid=99ccd395-af52-4a36-bca4-edd7991435bd).

b. Simulations

We use two experiments, a piControl and a 1pctCO$_2$ simulation. The piControl for CM2.6 is run for 200 years under 1860 preindustrial atmospheric forcing based on a constant globally averaged CO$_2$ mixing ratio of 286 ppm by volume (ppmv). The climate change simulation is an idealized $+1\%$ yr^{-1} CO$_2$ (1pctCO$_2$) rise experiment branched off from the piControl at year 121. Doubling of atmospheric CO$_2$ concentration occurs after 70 years of the simulation after which the concentration is held at 572 ppm for 10 years. The piControl experiment for CMIP5 is set to atmospheric concentrations of 286.15 ppmv, 790.9 ppbv, and 275.4 ppbv for CO$_2$, CH$_4$, and N$_2$O, respectively (Taylor et al. 2012). The same 1pctCO$_2$ simulation described for CM2.6 is used for all CMIP5 models. For the entire duration of the experiment, all non-CO$_2$ forcing agents (N$_2$O, tropospheric and stratospheric O$_3$, tropospheric sulfates, black and organic carbon, dust, sea salt, and solar irradiance) are held constant at values representative of year 1860. Only a single run (r1i1p1) is used for each CMIP5 model. Note that we use the piControl and 1pctCO$_2$ simulations, instead of the
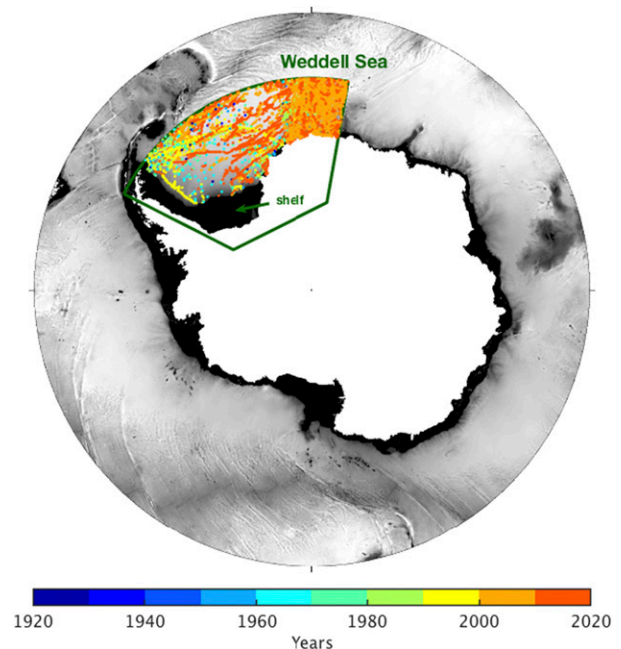

FIG. 1. Topography (gray shading) of the Southern Ocean (<55°S) depicting the Weddell Sea sector investigated in this study overlaid with positions and years of observations from the World Ocean Database spanning from 1912 to 2018.

historical and representative concentration pathway 8.5 (RCP8.5) simulations that are discussed in de Lavergne et al. (2014), to allow for a more direct comparison of the CMIP5 models with CM2.6 for which no historical or RCP8.5 simulation is available.

c. Observations

Observational profiles of temperature and salinity used in this study are from the World Ocean Database (WOD), spanning from 1920 to 2018 in the open-ocean Weddell Sea (Fig. 1; Boyer et al. 2018). This dataset corresponds to 16 071 profiles including observations from regional Argo floats, cruises, and instrumented elephant seals. All data are binned into a 0.25° × 0.25° grid. To avoid temporal bias, monthly anomalies are calculated for each year of observations by subtracting the appropriate monthly gridded WOCE/Argo Global Hydrographic Climatology (WAGHC; Gouretski 2018) from the gridded observational profiles. Yearly anomalies are then calculated as the mean of the monthly anomalies for each year. The yearly anomalies for each year are then added to the WAGHC annual climatological mean to produce a yearly temperature and salinity profile for each grid in the depth range from 0 to 2000 m following de Lavergne et al. (2014). We use the winter sea ice extent observations from the Hadley Centre Sea Ice and Sea Surface Temperature dataset (HadISST; Rayner et al. 2003), which span from 1970 to 2018; precipitation (liquid + snow) and evaporation fluxes from the ECMWF interim reanalysis (ERA-Interim), which span from 1979 and 2018 (Dee et al. 2011); and sea ice freezing
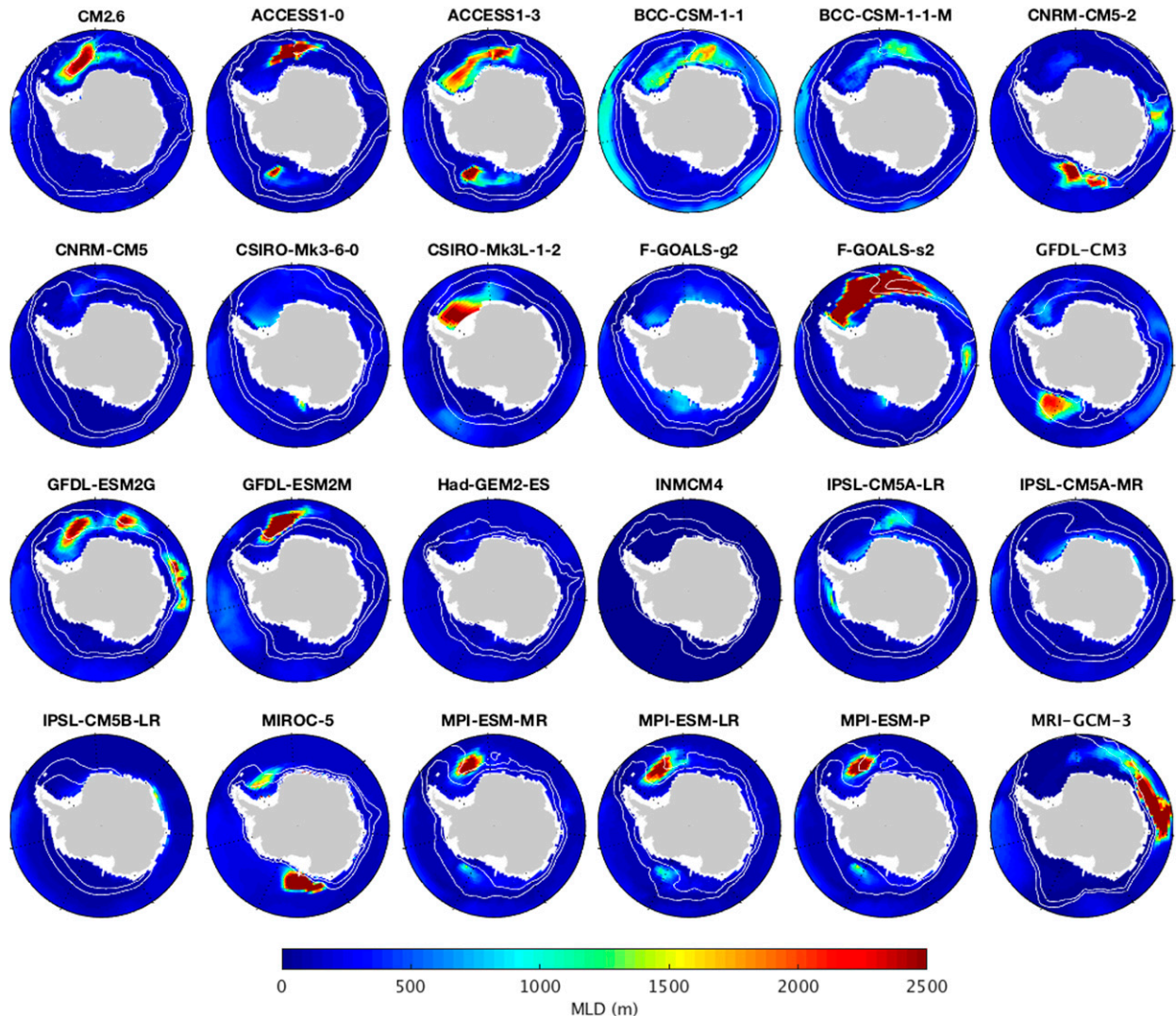
FIG. 2. Winter mixed layer depth (shading) and sea ice concentrations at 25% and 75% (white contours) averaged over the piControl experiment for all models analyzed. Winter averages are taken over July–September. The masked shelf region appears in white.

and melting flux from observational estimates described in Haumann et al. (2016), which are averaged between 1982 and 2008 and which we retrieved from a publicly available repository at https://www.envidat.ch/dataset/10-16904-8.

d. Domain of analysis

The focus of this study is on the western sector of the Weddell Sea, which we delimit in longitude by the Maud Rise and Antarctic Peninsula (63°W–10°E) and in latitude by the tip of the Antarctic Peninsula and Antarctic continent (63°–78.5°S; Fig. 1). This domain is chosen as open-ocean deep convection is predominantly observed in this sector of the Weddell Sea in both observations and models (Gordon 1978; Carsey 1980; Gordon 1982). For some models, the intensity of open-ocean deep convection events is sensitive to the northern and eastern boundaries of the domain, as convection can extend to the east of 10°E and north of 63°S (Fig. 2). However, the occurrence of

these events is not significantly affected by the choice of the domain. To take into account the polynyas developing outside of that domain (e.g., several models show convection in the Ross Sea), we also investigate convection over the whole Southern Ocean (<55°S; Fig. 1). To eliminate coastal polynyas from this study and to allow for comparison between the open and shelf regions, the domain of analysis is further divided into the open-ocean region and shelf region using the 1000-m isobath. This contour is chosen as the approximate location of the ASC (Dufour et al. 2017; Goddard et al. 2017).

In models, convection events are detected by examining the convection area, which is defined as the surface area where the September mixed layer depth (MLD) exceeds 2000 m, following de Lavergne et al. (2014). The MLD is determined using a threshold method based on density: $\sigma_\theta(z) - \sigma_\theta(\text{surface}) = 0.03\,\text{kg m}^{-3}$, where σ_θ is the potential density
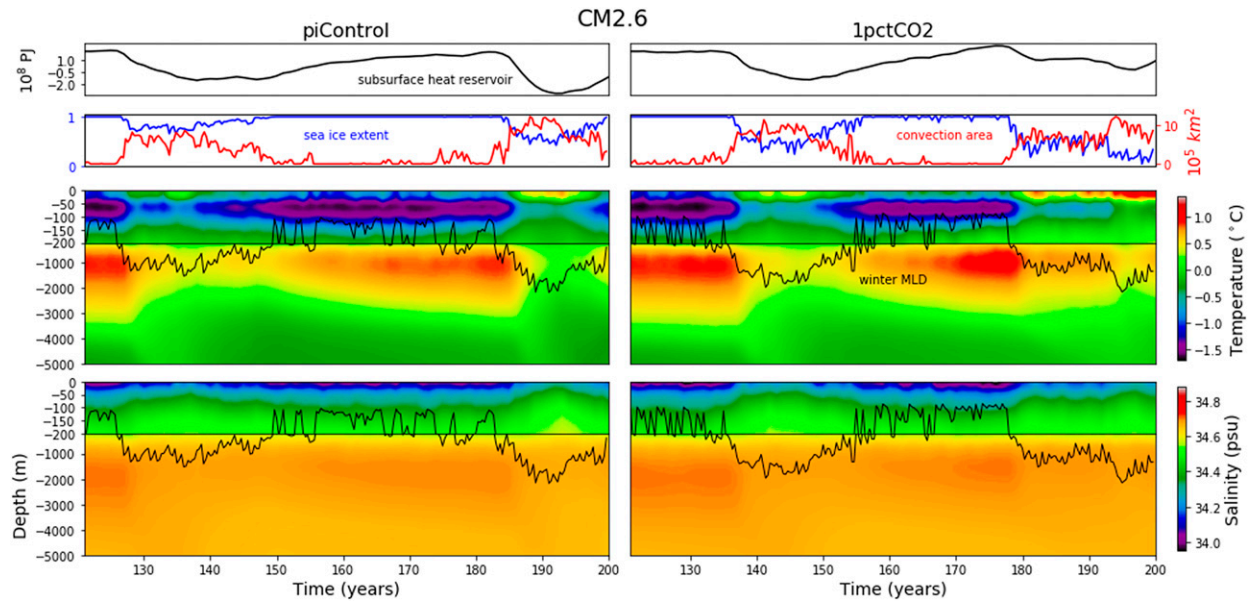
FIG. 3. Sea ice and thermohaline properties of CM2.6 (left) piControl and (right) 1pctCO$_2$ simulations averaged over the open-ocean Weddell Sea region (see section 2d and Fig. 1). The top panel contains time series of the subsurface heat reservoir (10^8 PJ) defined as the annual heat anomaly, relative to the average heat content over the entire control simulation, in the depth range of 200–2000 m. The second from top row contains the dimensionless winter sea ice extent (July–September; blue line) and September convection area (red line; section 2d). Sea ice extent is defined using a 15% sea ice concentration threshold. The two lower panels are Hovmöller diagrams (depth vs time) of annual mean potential temperature (°C) and salinity (psu) overlaid with time series of winter MLD in the open-ocean Weddell Sea (averaged over July–September; black line). Note that there is a zoom on the upper 200 m of the salinity and potential temperature fields. In addition, salinity and potential temperature fields are not fully saturated to allow for visual comparison with Fig. 4.

referenced to the surface (de Boyer Montégut et al. 2004). Convective models are models containing at least one year in either simulations where the average September convection area exceeds 10^5 km^2 (de Lavergne et al. 2014) in the Weddell Sea. For each model, the calculation of change under climate change (1pctCO$_2$ minus piControl) is carried out over the period corresponding to the longest consecutive nonconvective period during the 1pctCO$_2$ simulation between years 40–80. Using a fixed time period instead would lead to comparing polynya periods in some models with non-polynya periods in other models. This would be an issue as convection events and associated polynyas significantly impact the surface salinity and freshwater fluxes. The time periods used for each model are available in Table S1 in the online supplemental material.

3. Convection and the Weddell Sea Polynya in climate models

CM2.6 simulates two Weddell Sea convection events over both the piControl and 1pctCO$_2$ simulations, each of which result in the development of large open-ocean polynyas (Fig. 2). The relation between convection events and polynya formation in CM2.6 can be deduced from Fig. 3. Convection events are evident when convective area increases from near zero to above 8×10^5 km^2, with the MLD deepening from an average of approximately 150 to 1500 m. During each convection event, warm water is transported vertically from depth to the surface, resulting in the depletion of the subsurface heat

reservoir (for a definition see the caption of Fig. 3). The vertical transport of warm water to the upper ocean melts sea ice, decreasing the dimensionless winter sea ice extent from approximately 1 to 0.6, resulting in a polynya. Recharge of the subsurface heat reservoir of approximately 1–2 × 10^8 PJ then occurs, building up to the next convection event. The polynyas observed in CM2.6 are larger and occur over a longer duration compared to the Weddell Sea polynya observed in the 1970s (Fig. 4a).

CMIP5 models show substantial variability with respect to convection and polynya occurrence across the models (Figs. 2 and 4b–f). The frequency and duration of convective events in CMIP5 models are highly model dependent with most models showing continuous or quasi-continuous convective activity. The average Weddell Sea winter MLD in CMIP5 models is generally found at depths between 150 and 200 m, increasing to 1500–2000 m during convection events. Furthermore, convection events in CMIP5 models do not necessarily result in polynyas (Fig. 2). This point is most clearly evident in ACCESS1.0, where continuous convection is observed with no change in average winter sea ice concentration associated with a polynya (Fig. 4b). This disconnect between deep convection and polynyas warrants careful interpretation of results when discussing the occurrence of polynyas.

Although convection events in CMIP5 models are predominantly found in the Weddell Sea, convective regimes are observed for 10 models in the Ross Sea and for four in the Indian Ocean sector of the Antarctic (Fig. 2). Of the 23 CMIP5
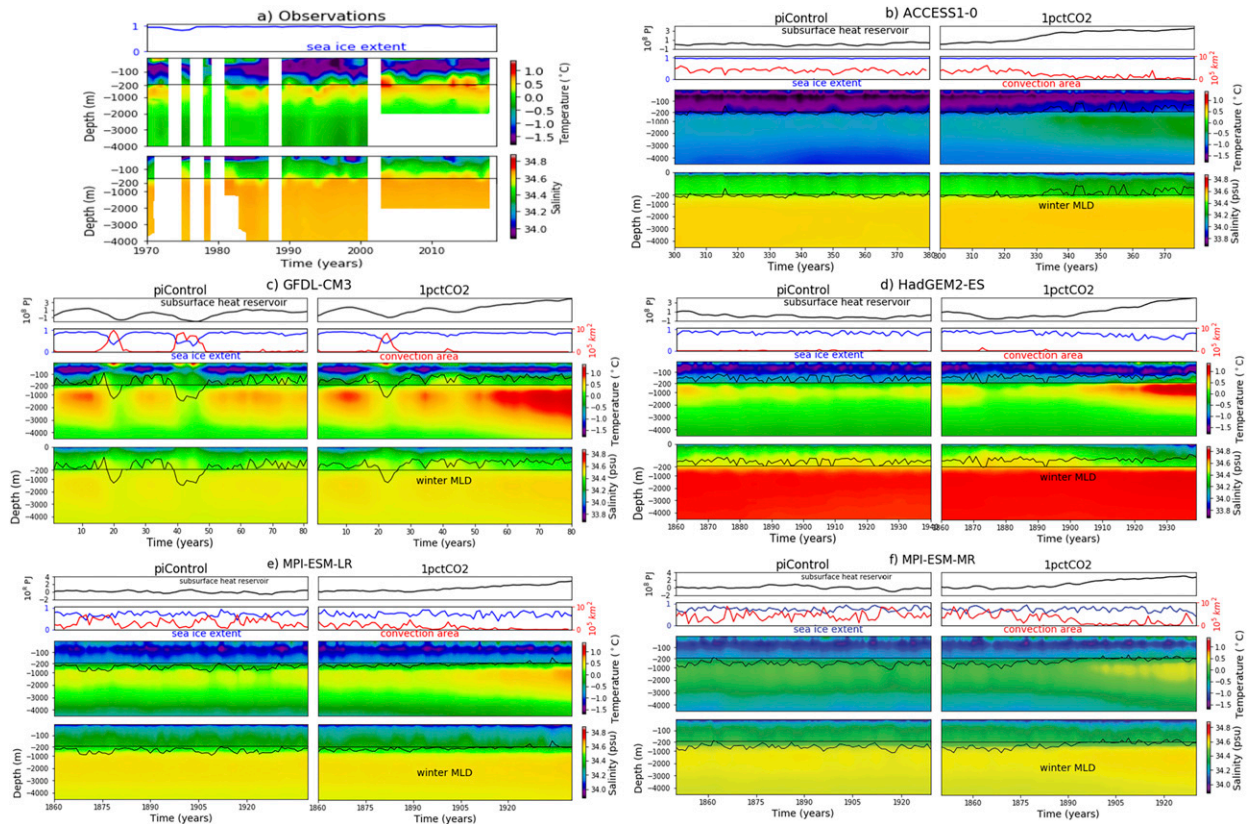
FIG. 4. (a) Sea ice and thermohaline properties for observations over the open-ocean Weddell Sea (see section 2c). The top panel contains time series of winter sea ice extent (July–September; blue line) from the Hadley Centre Sea Ice and Sea Surface Temperature dataset (HadISST; Rayner et al. 2003) from 1970 to 2018. Note that the start at 1970 is chosen to show the Weddell Sea polynya that occurred in 1974–76, but does not extend further back as the dataset prior to 1979 is of lower resolution and is less homogeneous (using multiple algorithms) compared to the current satellite period from 1979 onward. The two lower panels are Hovmöller diagrams (depth vs time) of annual mean potential temperature (°C) and salinity (psu) observations from the WOD spanning from 1970 to 2018 (see section 2c). The sea ice extent is defined using a 15% sea ice concentration threshold. White colors correspond to missing data. (b)–(f) As in Fig. 3, but for ACCESS1.0, GFDL-CM3, HadGEM2-ES, MPI-ESM-LR, and MPI-ESM-MR, respectively.

models used in this study, six models show no convection in the Weddell Sea (see Table 2), and out of these six models, four models (HAD-GEM2-ES, INM-CM4, IPSL-CM5B-LR, and IPSL-CMAB-MR) exhibit no convection in all regions. In the Weddell Sea, the majority of CMIP5 models have a mean convection area over the 80 years of piControl of between 1 and $4 \times 10^5 \, km^2$, while CM2.6 exhibits mean convection of $3.27 \times 10^5 \, km^2$ (Table S2).

The modeled subsurface heat reservoir, associated with a temperature maximum between 130- and 1600-m depth (Smedsrud 2005), in CMIP5 models and CM2.6 extends to approximately 1500 m, while in the observations the subsurface heat reservoir is shallower, extending to approximately 1000 m (Figs. 3 and 4). Significant discrepancies are visible in thermal structure between models and between models and observations (Fig. 4), with some models exhibiting either warmer (+0.5°C; Figs. 3 and 4c,d) or cooler (−0.5°C; Figs. 4b,f) temperatures associated with the subsurface heat reservoir compared to observations (Fig. 4a). Models with continuous or quasi-continuous convective activity generally simulate lower

temperatures in the subsurface heat reservoir (Figs. 4b,e,f) with mean temperatures in the depth range of 200–3000 m being approximately 0.5°C lower than observations (Fig. 4a). Overall, CM2.6 and most CMIP5 models agree on the magnitude and vertical structure of salinity with observations (Figs. 3 and 4). CM2.6, however, exhibits high salinity below 200 m by approximately 0.1 psu compared to observations (Figs. 3 and 4).

In the 1pctCO$_2$ simulation, all of the 17 convective CMIP5 models show a decrease in convection area in the Weddell Sea (Figs. 4 and 5; Table 2) with the multimodel mean linear regression trend in convection area of $-3.5 \times 10^4 \, km^2 \, decade^{-1}$ over the sensitivity experiment (Table 2). Out of all convective models, 10 show a full cessation (ACCESS1.0, BCC-CSM1.1, BCC-CSM1.1-m, CNRM-CM5, CNRM-CM52, CSIRO-Mk3L-1.2, GFDL CM3, IPSL-CM5A-LR, MPI-ESM-LR, MPI-ESM-P) in the Weddell Sea within the 80 years of simulation, while 7 show a slowdown (ACCESS1.3, FGOALS-s2, GFDL-ESM2G, GFDL-ESM2M, MPI-ESM-MR, MIROC5, MRI-CGCM3).

TABLE 2. Change per decade in convection area, surface salinity, and upper density stratification calculated from a linear regression over the full 1pctCO$_2$ experiment. The second group of CMIP5 models separated from the first by a blank line corresponds to the nonconvective models in the Weddell Sea. Convective models are models containing at least one year in either simulation where the average September convection area exceeds 10^5 km^2 (section 2d). The second to last column is the correlation coefficient between salinity and convection area. Bold values indicate significant linear trends to 95%. The last column shows the change (1pctCO2 minus piControl) in number of years of polynya. A polynya year is a year when average winter (July–September) sea ice extent falls below 85% of the piControl maximum sea ice extent. We detrended and applied a 5-yr running mean to the sea ice extent time series prior to detecting polynya years.

Model	Convection area ($10^4 \times$ km^2 decade^{-1})	Surface salinity ($\times 10^{-2}$ psu decade^{-1})	Density stratification ($\times 10^{-2}$ kg m^{-3} decade^{-1})	Correlation salinity and convection	Change in number of polynya years
CM2.6	3.5	0.94	0.045	**0.79**	8
ACCESS1.0	**−5.3**	**−2.5**	**1.3**	**0.80**	0
ACCESS1.3	**−3.5**	**−1.8**	**1.2**	**0.58**	0
BCC-CSM1.1	**−4.2**	**−0.91**	**0.58**	**0.81**	−6
BCC-CSM1.1-m	**−3.7**	**−3.9**	**1.9**	**0.69**	−10
CNRM-CM5	−0.23	0.76	**−0.79**	−0.23	−3
CNRM-CM52	−1.7	**−2.9**	**1.5**	**0.48**	−5
CSIRO-Mk3L-1.2	**−6.2**	**−1.5**	**91**	**0.78**	0
FGOALS-s2	**−13**	**−1.5**	**0.54**	**0.89**	0
GFDL CM3	**−1.4**	**−0.90**	**1.0**	**0.58**	−9
GFDL-ESM2G	**−3.3**	**−2.2**	**1.7**	**0.68**	−8
GFDL-ESM2M	**−2.3**	**−0.86**	**0.34**	**0.67**	−3
IPSL-CM5A-LR	**−0.66**	**−0.16**	**0.52**	**0.84**	−8
MPI-ESM-LR	**−3.5**	**−0.75**	**0.089**	**0.57**	−3
MPI-ESM-MR	**−6.8**	**−0.89**	**0.43**	**0.77**	0
MPI-ESM-P	**−3.8**	**−0.79**	0.14	**0.63**	−3
MIROC5	**−0.25**	**−0.58**	0.15	**0.62**	−5
MRI-CGCM3	**−0.13**	**−0.91**	**0.61**	**0.45**	2
CSIRO-Mk3.6.0	0	**−2.3**	**0.69**	0	0
FGOALS-g2	0	**0.57**	−0.13	0	0
HadGEM2-ES	−0.081	**−3.4**	**0.60**	0.23	0
INM-CM4	0	**1.1**	**0.99**	0	0
IPSL-CM5A-MR	0	0.17	0.35	0	0
IPSL-CM5B-LR	0	**−0.90**	0.15	0	0

Changes in modeled Weddell Sea polynya events are detected by determining the change in number of years of polynya between the piControl and 1pctCO$_2$ for each model in the open-ocean Weddell Sea (Table 2). A polynya year is a year when average winter (July–September) sea ice extent falls below 85% of the piControl maximum sea ice extent. We detrended and applied a 5-yr running mean to the sea ice extent time series prior to detecting polynya years. Under the 1pctCO$_2$ forcing, the number of years of polynya decreases for most CMIP5 models (Table 2). Models that show quasi-continuous or continuous convection do not produce polynya (Figs. 4b,e,f) and therefore show no change in number of polynya years (Table 2). Note that an increase in polynya years does not necessarily mean that there are more polynya events; it could also mean that the polynya lasts longer. This is the case for CM2.6, which simulates two polynyas in both simulations with the Weddell Sea polynya of the 1pctCO$_2$ lasting slightly longer than that of the piControl (Fig. 3).

The decline in convection intensity for CMIP5 models under the 1pctCO$_2$ simulation is associated with a decline in polynya occurrence for models that do form polynyas (see Fig. 4c and Table 2). The decline in convection area under the 1pctCO$_2$ simulation in CMIP5 models is in good agreement with the results found by de Lavergne et al. (2014), despite using different climate change projections (section 2b). In contrast, the timing, duration, and intensity of polynya and convection events in CM2.6 under the 1pctCO$_2$ simulation are similar to that of the piControl simulation (Figs. 3 and 5).

4. Response of stratification to climate change

Episodic large deep convection events in the Weddell Sea have been linked in particular to anomalies in the southern annular mode index (Gordon et al. 2007; Cheon et al. 2014; Francis et al. 2019; Campbell et al. 2019; Cheon and Gordon 2019) and in the stratification of the upper ocean (Gordon et al. 2007; Campbell et al. 2019; Cheon and Gordon 2019), making wind and stratification two potential candidates to explain differences in convection response between CMIP5 and CM2.6 models. Misrepresentation of
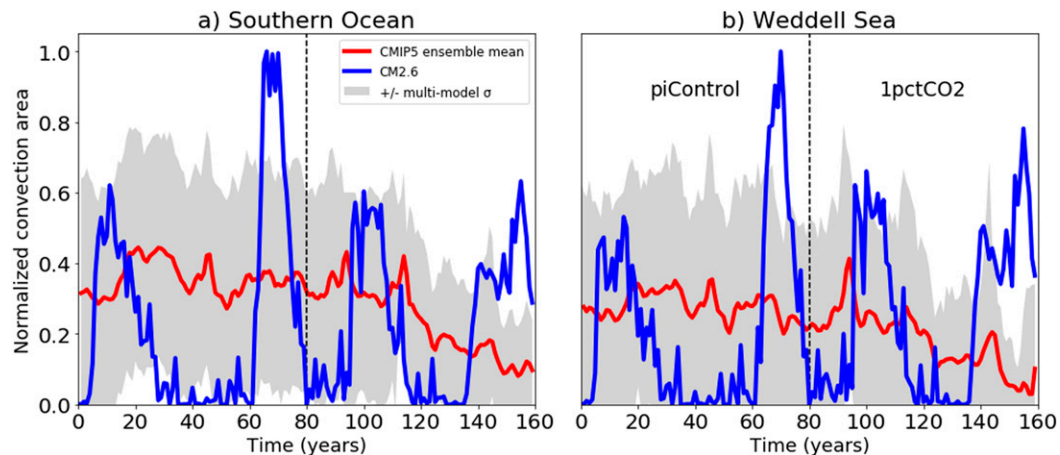
FIG. 5. Normalized convection area for the CMIP5 model mean (red) and CM2.6 (blue) for the open ocean of (a) the Southern Ocean and (b) the Weddell Sea. The gray shading denotes ±1 standard deviation across the CMIP5 models. For each model, the area is normalized by the maximum areal extent of convection recorded over all simulations for that model. The first 80 years denote the piControl, while the following 80 years (years 80–160) denote the 1pctCO$_2$simulation. The CMIP5 model mean (red) and CM2.6 model (blue) lines are computed as a 5-yr running mean.

the wind (e.g., Swart and Fyfe 2012; Bracegirdle et al. 2013) and of stratification (e.g., Sloyan and Kamenkovich 2007; Meijers 2014; Beadling et al. 2019) are very well known in climate models at those latitudes. The position and magnitude of the maximum zonal wind stress over time are very similar between CM2.6 and CMIP5 models under both the piControl and 1pctCO$_2$ simulations, with a typical equatorward bias in the maximum westerly position and weak bias in westerly strength relative to observations (Fig. S1a), as documented in detail in previous studies of CMIP5 models (e.g., Swart and Fyfe 2012; Bracegirdle et al. 2013). The change in strength and latitude of the maximum westerly position for CM2.6 falls within one standard deviation of that of the CMIP5 mean (Figs. S1b,c). These similarities between CM2.6 and CMIP5 models allow us to postulate that the change of the Southern Hemisphere westerlies during the 1pctCO2 simulation is likely not the main cause of the continuation of convection in CM2.6 under the 1pctCO$_2$ simulation as compared to CMIP5 models. We next explore the role of stratification on convection area.

A relatively weak vertical stratification, which is controlled by salinity from the surface to approximately 2000 m, regulates convection and polynya occurrence in the Weddell Sea in both observations (Campbell et al. 2019; Cheon and Gordon 2019) and climate models (Martin et al. 2013; de Lavergne et al. 2014; Stössel et al. 2015; Dufour et al. 2017). The majority of convective models have an average piControl vertical potential density difference (density at 2000 m minus at 10 m) between 0.3 and 0.4 kg m^{-3} and an average surface salinity between 34.0 and 34.3 psu, while observations exhibit an average potential density difference and surface salinity of 0.46 kg m^{-3} and of 34.3 psu, respectively (Fig. 6). In the piControl simulation, models with large average convective activity in the Weddell Sea

generally have weaker density stratification and higher surface salinity (0–100 m) compared to models with low average convection area (Fig. 6).

For 16 of the 17 convective CMIP5 models in the Weddell Sea, the slowing of convection activity in the 1pctCO$_2$ simulation coincides with surface freshening and an increase in vertical density gradient (Fig. 6). CMIP5 models exhibit a multimodel mean linear regression in open-ocean surface salinity of −0.011 psu decade^{-1} and in vertical potential density difference of 0.045 kg m^{-3} decade^{-1} over the sensitivity experiment in the Weddell Sea (Table 2). CNRM-CM5 is the only convective model that shows a decrease in density stratification and increase in surface salinity in response to the 1pctCO$_2$ simulation in spite of a decrease in convection area (Fig. 6). While the cause of CNRM-CM5 response to the 1pctCO$_2$ forcing is unclear, we note that this model is unique within the CMIP5 model group investigated in that it has a very strong Weddell Deep Water temperature bias of approximately +1°C compared to the group average. All convective models, except CNRM-CM5, exhibit strong and significant positive correlations ($r = 0.45$–0.89) between surface salinity and convection area under the 1pctCO$_2$ simulation (Table 2).

In contrast to the CMIP5 models, there is no significant difference in the open-ocean surface salinity or in the vertical potential density gradient between the piControl and the 1pctCO$_2$ simulations for CM2.6 (Table 2). CM2.6 simulates a very small increase in open-ocean potential density stratification, surface salinity, and convection area within the Weddell Sea in the 1pctCO2 compared to the piControl (Fig. 6). Over the CM2.6 1pctCO2 simulation, the change in surface salinity (−0.06 psu) and convection area (0.41 × 10^5 km^2) in the Weddell Sea is within one standard deviation of the piControl surface salinity (0.06 psu) and convection area (3.68 × 10^5 km^2). Hence, in the Weddell Sea, these
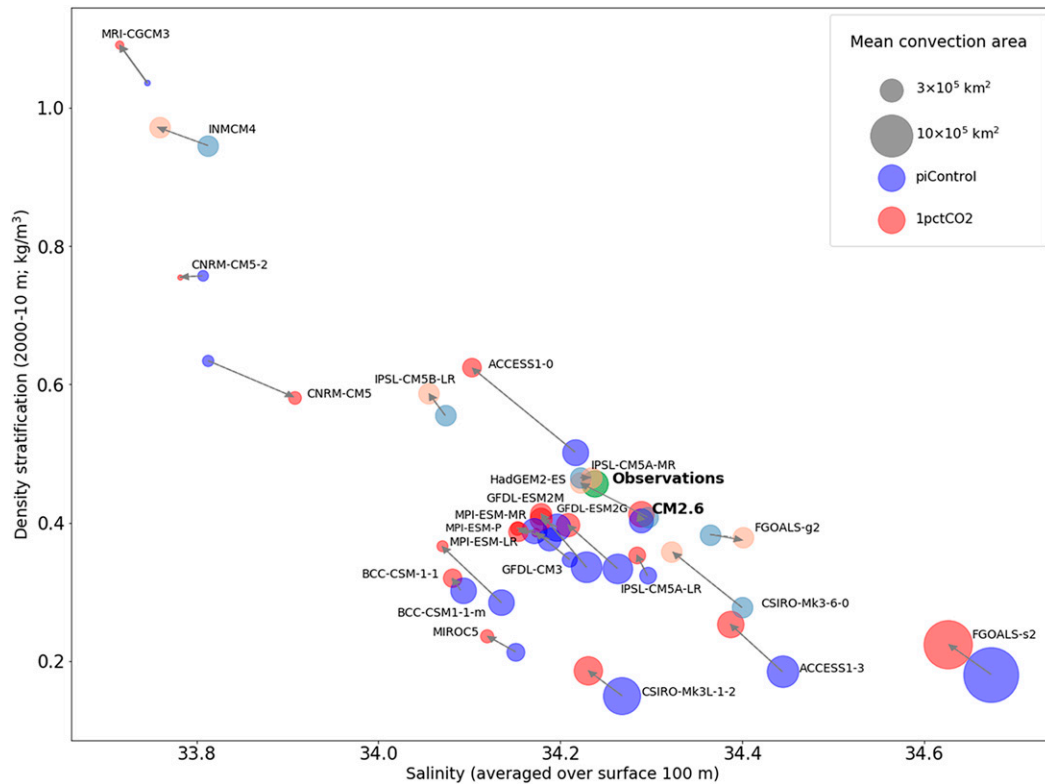
FIG. 6. Mean convection area over the piControl (blue) and 1pctCO$_2$ (red) simulations in the open-ocean Weddell Sea as a function of their respective annual surface salinity over the top 100 m and annual density stratification (from 2000 to 10 m density difference). Pale colored models correspond to nonconvective models in the Weddell Sea, defined as models that do not have a year where the September convection area exceeds 10^5 km^2. Averages are calculated over the full 80 years of each simulation as not all models convect during the same periods. Observations (green) are plotted with the average convection area of the 1970s Weddell Sea polynya and average salinity and density stratification of the WOD profiles spanning from 1920 to 2018. Most CMIP5 models undergo an increase in stratification in response to the 1pctCO$_2$ forcing (visible by the arrow pointing up), concurrent with a decrease in surface salinity (arrows pointing to the left) and decrease in convection are (larger blue than red circles).

changes cannot be distinguished from the model's natural variability of surface salinity and convection area.

In summary, when subject to the 1pctCO$_2$ forcing, CM2.6 responds with a statistically insignificant increase in convection area, density stratification, and surface salinity. CMIP5 models, in contrast, show a statistically significant slowdown, or even cessation, of convection events in the 1pctCO$_2$ simulation associated with an increased stratification and surface freshening. This surface freshening has been suggested to be mainly driven by freshwater forcing (de Lavergne et al. 2014; Stössel et al. 2015). Next, we explore the response of freshwater forcing to climate change.

5. Surface water fluxes and freshening

In the CMIP5 and CM2.6 models, total freshwater transport into the ocean is the net transport of liquid and frozen water entering the ocean and is the sum of the contribution from precipitation, evaporation, sea ice (melting and freezing), and

runoff (river runoff and iceberg calving). In all models, the freshwater transport entering the ocean from precipitation and evaporation intensifies toward lower latitudes in the piControl run, reaching its maximum at approximately 50°S (Figs. 7a,c). This modeled freshwater transport shows a low bias relative to that from ERA-Interim (Figs. 7a,c). In piControl, freshwater transport arising from sea ice melting and freezing exhibits large negative zonal values at high latitudes (>60°S) due to the predominance of sea ice formation in the vicinity of the continent in good agreement with observational estimates (Haumann et al. 2016; Fig. 7e). Models generally show a similar pattern in freshwater transport arising from iceberg calving and river runoff, but CM2.6 shows significantly larger transport than the multimodel mean of CMIP5 models, in particular between 65° and 70°S (Figs. 7g,i). We note that the spread in freshwater transport is large across CMIP5 models except for precipitation and evaporation. Overall in piControl, the total freshwater transport into the ocean is similar in pattern and magnitude between CM2.6 and most CMIP5 models, with

CM2.6 transport being around 35% larger than that of CMIP5 multimodel mean between 65° and 45°S (Fig. 7k).

In the 1pctCO$_2$ simulation, CMIP5 models and CM2.6 demonstrate an increase in total freshwater transport into the ocean between 80° and 50°S (Fig. 7l). South of 60°S, this increase can be attributed predominately to a combination of changes in sea ice, icebergs, and river fluxes (Figs. 7f,h,j). Between 60° and 50°S, the increase results from changes in precipitation, evaporation, and sea ice. This enhanced input of freshwater into the upper ocean under the 1pctCO$_2$ simulation contributes to lower surface salinity as seen in section 4.

In CMIP5 models, the change in total freshwater transport into the ocean in the Weddell Sea sector is 0.036 (σ = 0.030) Sv over the continental shelf and 0.015 (σ = 0.038) Sv in the open ocean (Fig. S2e). In CM2.6, this change is 0.082 Sv over the continental shelf and 0.034 Sv in the open ocean in the Weddell Sea. Hence, over the Weddell Sea shelf the change in CM2.6 is significantly larger than that of the CMIP5 multimodel mean (Figs. S2b,e). When the total freshwater transport change over the shelf is divided by the total shelf area in each model, CM2.6 is well within a standard deviation of CMIP5 models (Fig. S2f). Thus, CM2.6 shows a similar input of freshwater per area over the shelf regions, but an enhanced total freshwater transport due to its larger shelf region compared to the coarse-resolution models. In the open-ocean Weddell Sea, the change in CM2.6 is above the CMIP5 multimodel mean but within one standard deviation of that in the CMIP5 model ensemble (Figs. S2b,e). Additionally, the spatial distribution of change in freshwater flux into the ocean is similar between CM2.6 and CMIP5 models (Figs. S3g–l), with the largest changes in total freshwater transport into the ocean along the shelf regions. Hence, we rule out the hypothesis of a lack of freshening due to insufficient surface freshwater input in CM2.6 to explain the continued convection in that model.

In response to the 1pctCO$_2$ forcing, both the shelf and open-ocean regions of the Weddell Sea freshen over the top 50 m of the ocean in 18 of the CMIP5 models with different magnitude across models (Figs. 8b–f and Fig. S4). CM2.6 exhibits one of the largest depth averaged freshening in the Weddell Sea shelf region of all CMIP5 models but limited salinity change in the open ocean (−0.06 psu; Figs. 8a–f and Fig. S4). Yet, as we saw, freshwater input across the surface in CM2.6 is well within the range of that of CMIP5 models in the open-ocean region. The shelf versus open-ocean distribution of freshening in CM2.6 indicates a retention of the anomalous freshwater on the shelf. This geographical confinement of the freshening anomaly on the shelf suggests the existence of a dynamical barrier that prevents freshening from spreading offshore. Such a barrier could be provided by the ASC and ASF that are known to hamper cross-shelf transport (Jacobs 1991; Thompson et al. 2018). We investigate this hypothesis next.

6. Control of freshwater anomalies by the ASC and ASF

CM2.6 exhibits a strong westward ASC, consisting of numerous zonal jets with time average velocities exceeding 0.2 m s^{-1} in the Weddell Sea (Fig. 8g). While the ASC is present all around Antarctica in CM2.6, it is generally weak or absent along the West Antarctic Peninsula and in the Bellingshausen Sea (Fig. 8g) in agreement with observations (Thompson et al. 2018). Observed gradients in water mass properties are very strong across the ASC, between the cool and fresh shelf waters and the warmer and saline open-ocean Circumpolar Deep Water, with this gradient forming the ASF (Whitworth et al. 2013). In CM2.6, the ASC is accompanied by a strong ASF, as evident by prominent cross-shelf density, temperature, salinity, and sea level gradients (Figs. S5a–d). Additionally, the ASF manifests through strong isopycnal doming toward the continental shelf in CM2.6 (Figs. 9b,h,n). This strong ASF constrains the coastal freshening to remain close to the coast (Figs. 10a,f,k).

In the coarser-resolution CMIP5 models, current speeds in proximity to the Antarctic continent rarely exceed 0.05 m s^{-1} (Figs. 8h–l). Most CMIP5 models do not explicitly resolve continental shelf bathymetry and as a result do not show any lateral gradients in salinity or ASF (Figs. 9c–f, i–l, and o–r). The poor representation of the transition between the shelf and open-ocean regions in most CMIP5 models leads to the spreading of climate warming–induced freshwater anomalies away from the coast and into the open ocean (Figs. 10b–e, g–j, and l–o).

MPI-ESM-MR, which has a finer horizontal ocean grid spacing (0.4° × 0.4°) than the other CMIP5 models analyzed, has a more coherent ASC with higher depth averaged speed than the coarser-resolution CMIP5 models (Figs. 8h–l). However, this model does not show a strong retention of freshwater originating from the shelf (Figs. 10b,g,l), likely due to the relatively coarse resolution of the continental shelf bathymetry (Figs. 9c,i,o). The weak ASF retention allows the additional freshwater to spread in the open ocean, likely contributing to the slowdown in open-ocean convection similar to that found in the other CMIP5 models. A comparison between MPI-ESM-MR and its coarser-resolution counterpart MPI-ESM-LR shows a weaker total water transport into the ocean in MPI-ESM-MR than in MPI-ESM-LR (Fig. S2e); however, MPI-ESM-MR has higher surface freshening than MPI-ESM-LR as the freshwater input is mixed further down in the water column and transported farther offshore in MPI-ESM-LR in the Weddell Sea (Figs. 10l,m). The enhanced near-surface retention of freshwater anomaly in MPI-ESM-MR as compared to MPI-ESM-LR supports the hypothesis of constraining of freshening by the ASF and ASC as horizontal resolution increases (Figs. 10g,h,l,m).

Hence, in CM2.6, the retention of freshwater anomalies on the shelf would lead to a very modest change in salinity in the open-ocean region of the Weddell Sea that would not prevent the continuation of the deep convection events and associated polynyas. In contrast, in CMIP5 models, the limited spatial distinction in freshening and density changes between the shelf and open-ocean regions suggests that freshwater anomalies spread from the shelf to the open ocean contributing to a reduction of open-ocean convection (Figs. 8b–f).

7. Discussion

a. Representation of the ASF and ASC in models

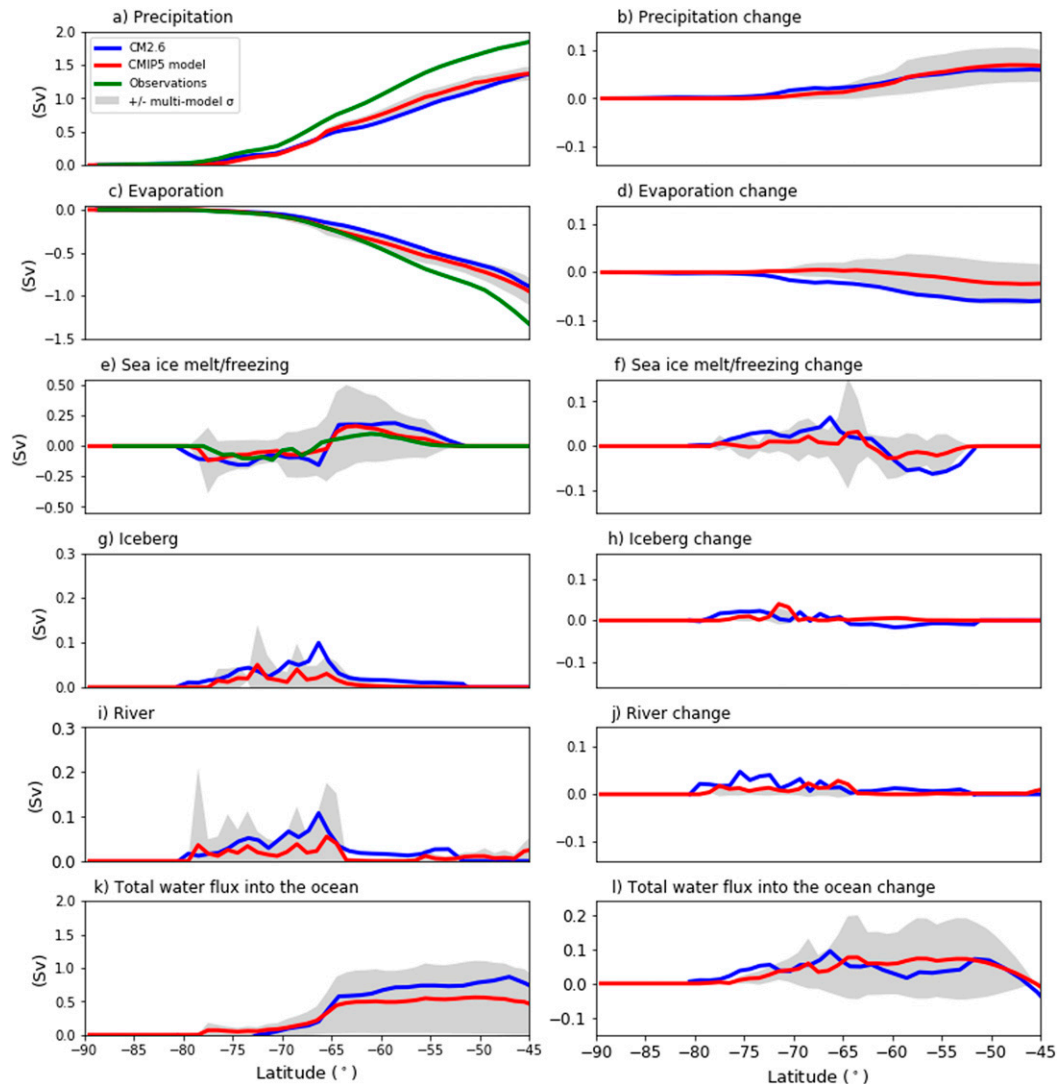Despite generally exhibiting a high transient climate response over the 1pctCO$_2$ simulation compared to CMIP5

FIG. 7. Freshwater transport (Sv) into the ocean (left) in the piControl simulations and (right) in response to climate change (1pctCO$_2$ minus piControl) for CM2.6 (blue) and the CMIP5 model mean (red). The transport is calculated as the zonally integrated water flux into the ocean (wfo output) and is binned into 1° latitude bins. The total freshwater transport shown in (k) and (l) is the sum of transports from (a),(b) liquid and solid precipitation, (c),(d) evaporation, (e),(f) sea ice melting/freezing, (g),(h) iceberg calving, and (i),(j) river runoff. For comparison with models (green), we show precipitation and evaporation in (a) and (c), respectively, averaged between 1979 and 2018 from ERA-Interim reanalysis (Dee et al. 2011; see section 2c), and sea ice freezing and melting flux in (e) averaged between 1982 and 2008 from observational estimates described in Haumann et al. (2016) (see section 2c). Positive values denote a positive flux into the ocean. Not all variables were available for the 23 CMIP5 models used in this study. The models used to compute the CMIP5 models means (red) and standard deviations (gray shades) for each panel are listed in Table S3. CMIP5 model precipitation and evaporation fluxes in (a)–(d) are for all 23 CMIP5 models used in this study. All calculations are made over the time period indicated in Table S1.

models (Winton et al. 2014; see section 2a), the occurrence and intensity of convection events in the high-resolution CM2.6 is found to be largely unchanged between the piControl and 1pctCO$_2$ simulations. Namely, its change in open-ocean salinity and convection area are indistinguishable from natural variability represented by the piControl. The ASF acting as a barrier to the transport of freshwater away from the shelf in

CM2.6 likely contributes to the absence of a significant change in response to the 1pctCO$_2$ forcing in that model. To help assess the integrity of the modeled ASF and ASC in CM2.6 and CMIP5 models, we here compare them to that from the LLC_ 4320 model [Stewart et al. 2019; section 2a(3)].

Comparison between CM2.6 piControl and LLC_4320 reveals general agreement in ASC velocity and ASF frontal
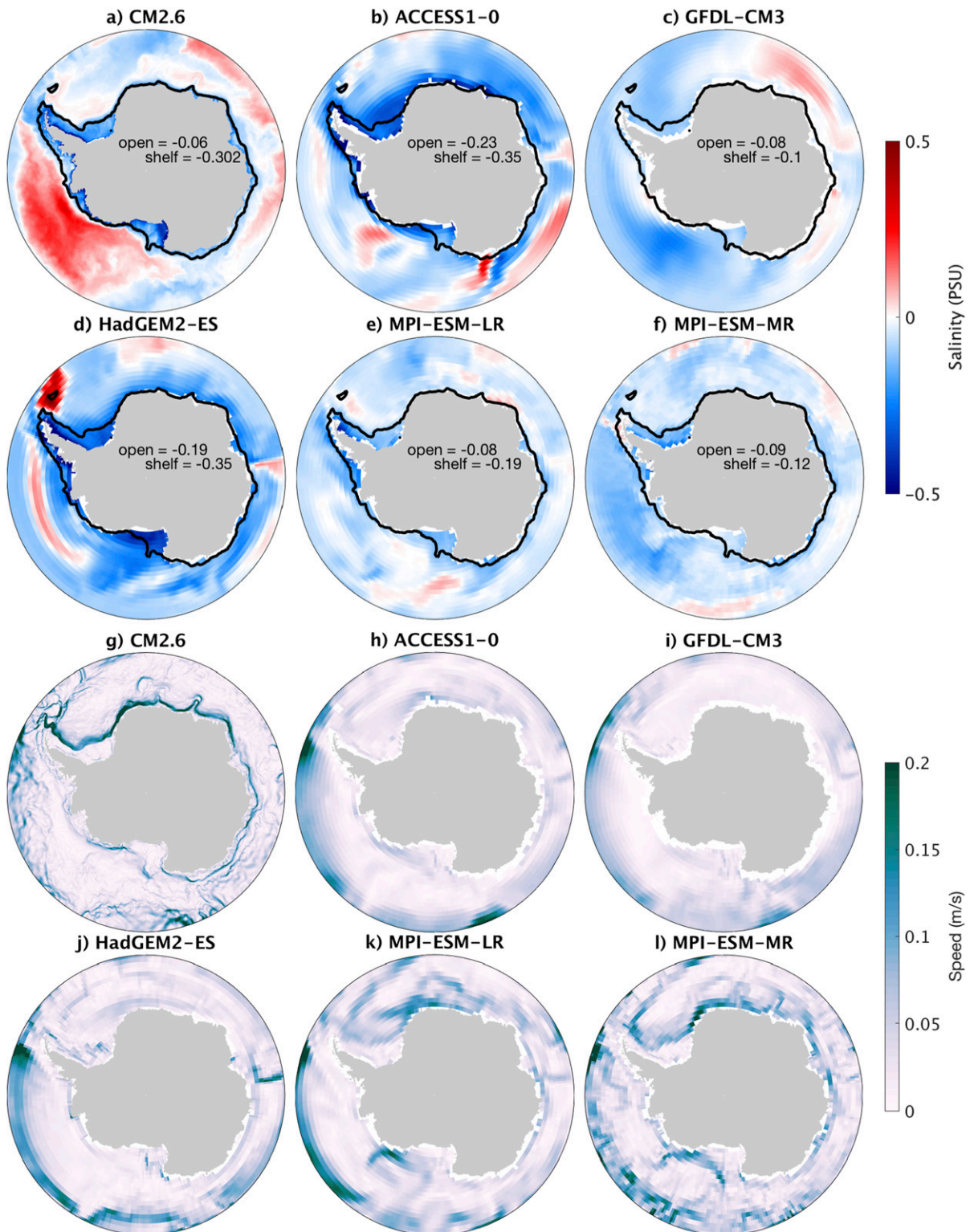
FIG. 8. (a)–(f) Salinity change (1pctCO$_2$ minus piControl) averaged over the top 50 m, and 1000-m isobath (black contour) for CM2.6 and a subset of the 23 models. Numbers over the continent correspond to the top 50-m depth averaged salinity change (lower number) in the shelf region and (upper number) in the open-ocean region of the Weddell Sea. (g)–(l) Speed averaged over the top 1000 m in the piControl simulation for CM2.6 and a subset of the 23 models.
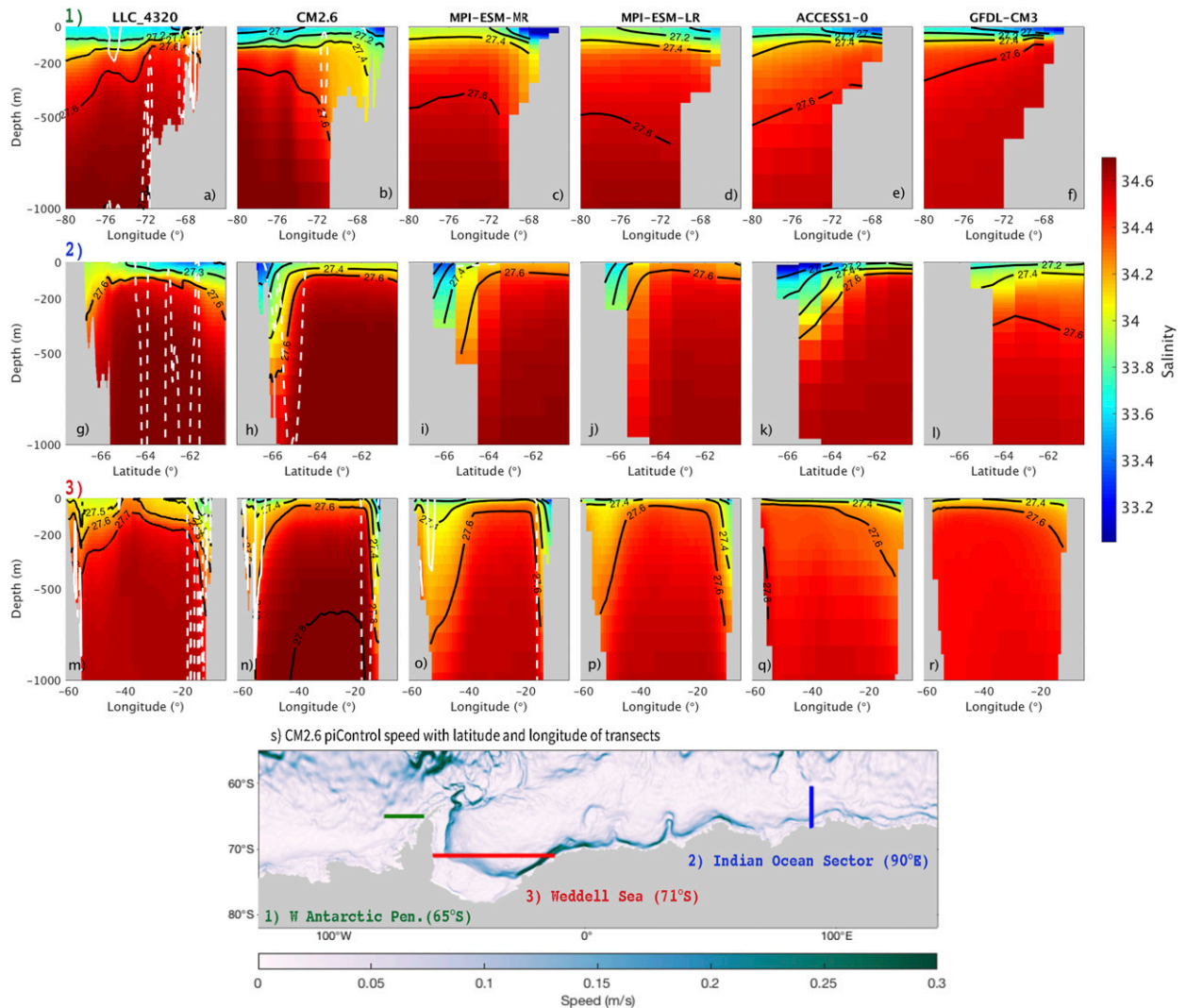
FIG. 9. Salinity cross sections at (first row) 65°S, (second row) 90°E, and (third row) 71°S for (a),(g),(m) LLC_4320 and for the piControl simulation of (b),(h),(n) CM2.6 and of a subset of the 23 CMIP5 models: (c),(i),(o) MPI-ESM-MR, (d),(j),(p) MPI-ESM-LR, (e),(k),(q) ACCESS1.0, and (f),(l),(r) GFDL CM3. A justification for the position of the transects can be found in section 7a. In (a)–(r) black contours correspond to potential density referenced to the surface (σ_0; kg m^{-3}) and white contours to ± 0.08 m s^{-1} zonal velocity contours (m s^{-1}). (q) Average speed (0–1000 m) in the piControl simulation of CM2.6 and transects used for the salinity cross sections.

structure (Figs. 9a,b,g,h,m,n). In the Weddell Sea region, heavier density classes are able to access the shelf region in LLC_4320, whereas stronger isopycnal doming toward the continent in CM2.6 isolates the lower shelf region from the open ocean (Figs. 9m,n). At the surface, CM2.6 and LLC_4320 have similar ASF structures, with fresh shelf water limited to approximately the same extent across the shelf (Figs. 9m,n). In contrast, most CMIP5 models are unable to capture the ASC and the associated ASF (Figs. 9c–f, i–l, and o–r).

Although there is an overall agreement between CM2.6 and LLC_4320, the ASF and ASC in CM2.6 may be too strong compared to observations as argued in Goddard et al. (2017), which would lead to a too strong retention of freshwater over the shelf region. The too strong ASF and ASC in CM2.6 may be due to underrepresented mesoscale eddy activity, which, if

resolved, would flatten isopycnals akin to the LLC_4320 simulation. CM2.6 may also simulate a too laminar ASF and ASC, which may lead to an overly strong dynamical barrier, whereas a more turbulent flow would allow the emission of mesoscale eddies, hence contributing to the lateral transport of surface freshwater anomalies (Stewart and Thompson 2015). In addition to mesoscale eddies, tides and dense overflows are thought to be critical components of cross-slope and cross-shelf exchange (Thompson et al. 2018). Strong tides in the central Weddell Seas should subdue cross-slope exchange, whereas the weaker tidal amplitudes in the western Weddell Sea should intensify cross-slope exchange (Beckmann and Pereira 2003; Thompson et al. 2018). Dense water overflows directly affect the overlying stratification associated with the ASF (Baines 2008). In CM2.6, dense water overflows are weak and do not
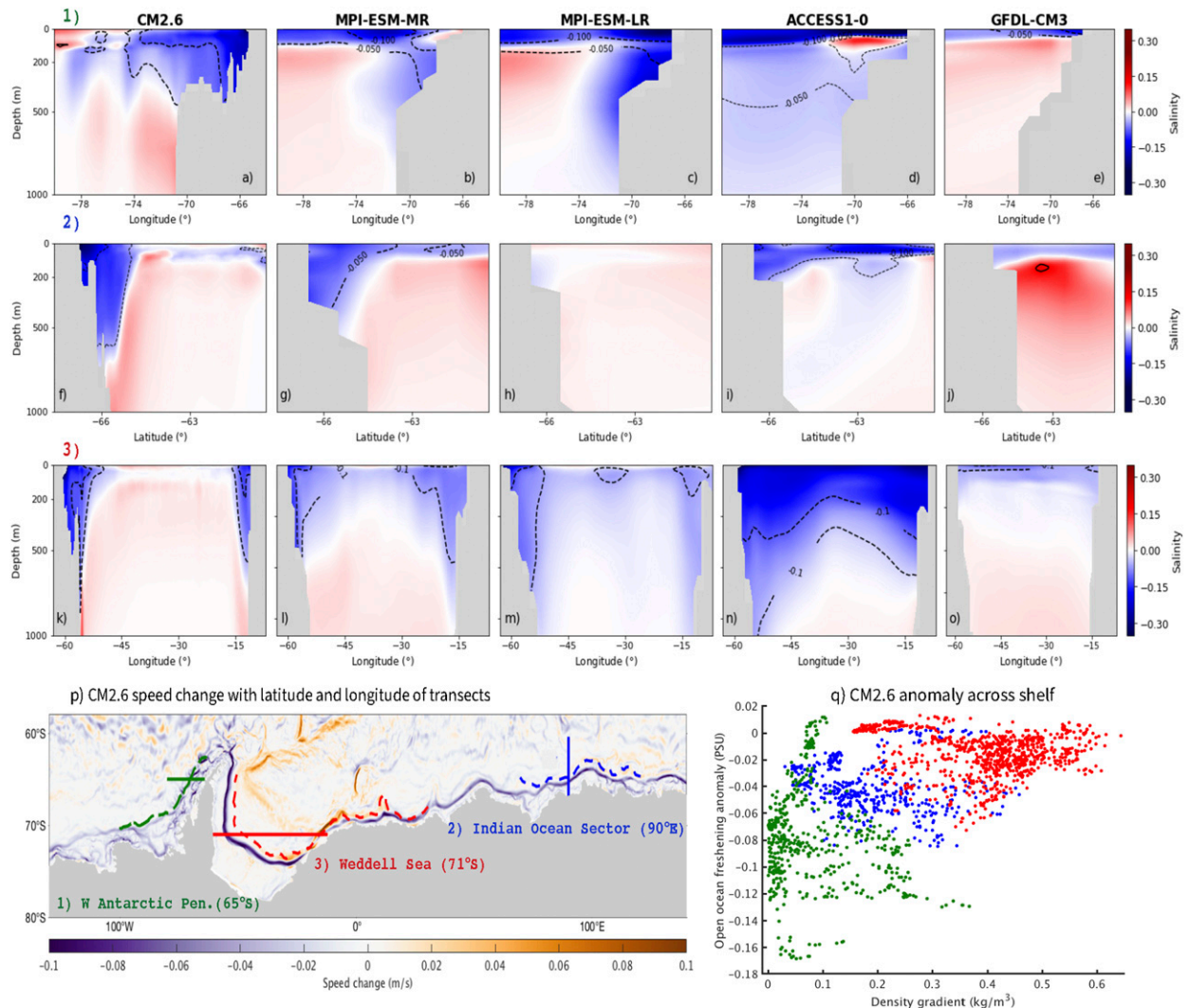
FIG. 10. (top three rows) As in the top three rows of Fig. 9, but for salinity change (1pctCO$_2$ minus piControl). Note that the LLC_4320 model is not displayed as this model does not have any corresponding climate change simulation. (p) Average speed (0–1000 m) change in CM2.6 and transects used for the salinity cross sections. A justification for the position of transects can be found in section 7a. (q) Scatterplot of cross-shelf density gradients in the piControl (as a measure of the ASC strength) vs salinity change (1pctCO$_2$ minus piControl) in the open ocean in CM2.6. Calculations are made over the top 150 m, with gradients calculated as the difference between the 0–800- and 3000–3400-m isobaths. Open-ocean salinity is calculated over the top 150 m and in the 3000–3400-m isobaths. In strong ASC regions, such as the Weddell Sea (red dots), we see large density gradients associated with weak open-ocean freshening. Each point in (q) is calculated at each grid point for CM2.6 along the dashed lines (1300-m isobath) in (p).

exceed 1500 m, due to insufficient resolution on the horizontal leading to underrepresentation of mesoscale eddies and fine-scale topography (Dufour et al. 2017) and insufficient resolution on the vertical that does not allow for resolving dense downslope flow scales (Winton et al. 1998). Lack of full representation of mesoscale eddies, tides, and dense water overflows may therefore alter the ability of CM2.6 to realistically capture the ASF and associated cross-shelf freshwater exchange.

Even so, the general congruence between CM2.6 and LLC_4320 on the representation of the ASF, in particular near the surface, and the inability of CMIP5 models in simulating the ASF and ASC suggest that CM2.6 may be closer to reality than

CMIP5 models. If so, convection and the associated Weddell Sea polynya under climate change may well continue into the future as suggested by CM2.6 simulations, although the frequency and/or duration of the events could be altered. As only one member of each simulation is used in this analysis, caution should be taken in drawing any definitive conclusion. In particular, ensemble members run over longer time period would be needed to separate natural variability from the forced signal, and hence to confirm our results. Running large ensemble members of CM2.6 model is currently beyond modeling centers computational capabilities. Furthermore, a longer simulation of CM2.6 would be needed to determine whether the

convection events continue unaffected or are eventually modified by the change in forcing under a climate change simulation. Finally, the variety of models used prevents us from drawing firm conclusions. A controlled framework should be used to isolate the role of the ASF and ASC on convection. While this paper highlights an important mechanism for controlling the current and future occurrence of polynyas, other mechanisms that have been shown to significantly affect convection (Martin et al. 2013; Heuzé et al. 2013; Reintges et al. 2017; Cheon and Gordon 2019) and its response to climate change (Heuzé et al. 2015) could also play a significant role in explaining the difference between the two categories of models analyzed.

b. Relation between ASC strength and open-ocean freshening

Our results suggest that in the future, freshening at the surface of the open-ocean region around Antarctica may be constrained in scope by the ASF and ASC. Yet, some freshening may be expected in regions with an absence of the ASF and ASC. Following Thompson et al. (2018), we identify three regions of differing ASF character and ASC strength in the piControl of CM2.6:

1) The West Antarctic Peninsula (65°S) where the ASC is weak (<0.05 m s^{-1}; Fig. 9s) and speed change under the 1pctCO$_2$ simulation is weak ($<|0.03|$ m s^{-1}; Fig. 10p). There, the freshening signal spreads beyond the shelf region at most depths (Fig. 10a), and weak cross-shelf density gradients are associated with large offshore freshwater anomalies (green points in Fig. 10q).
2) The Indian Ocean sector (90°E) where the ASC is moderate (~ 0.1 m s^{-1}; Fig. 9s) and speed change under the 1pctCO$_2$ simulation is moderate ($|0.03|$–$|0.06|$ m s^{-1}; Fig. 10p). There, the moderate to strong cross-shelf density gradients act to constrain freshening at most depths (Fig. 10f), and are associated with relatively weak offshore freshwater anomalies (blue points on Fig. 10q).
3) The Weddell Sea (71°S) where the ASC is strong (>0.1 m s^{-1}; Fig. 9s) and speed change under the 1pctCO$_2$ simulation is strong ($>|0.06|$ m s^{-1}; Fig. 10p). There, the freshening is strictly constrained to the shelf region with little surface propagation of freshwater to the open ocean (Fig. 10k; see section 4), and large cross-shelf density gradients are associated with weak offshore freshwater anomalies (red points in Fig. 10q).

Spreading of the freshening signal in the absence of the ASF and ASC supports the mechanism proposed here in which, where the ASF and ASC are strong, freshening over the shelf does not spread to the open-ocean region. This implies that, in sectors of the Southern Ocean offshore of regions with a weak or absent ASF and ASC, a substantial decrease in salinity might be expected due to increased freshwater input on the shelf. In the absence of a dynamic barrier at the shelf break, this freshwater would propagate toward the open ocean. Anomalous freshwater over the shelf predominately results from enhanced iceberg and river transport from the Antarctic continent, and from changes in sea ice freezing/melting, as shown in section 5.

Similarly to Antarctic shelf circulation, strong boundary currents, including the East Greenland Current, West Greenland Current, and Baffin Island Current, are found along the shelves of the polar northwest Atlantic (Lazier and Wright 1993). These boundary currents carry cold and freshwater and play a major role in mediating the transport of freshwater between the shelf and the open ocean (Marsh et al. 2010; Weijer et al. 2012; Dukhovskoy et al. 2016). Enhanced freshwater fluxes due to a melting Greenland ice sheet (Bamber et al. 2012; Enderlin et al. 2014) and changes in Arctic outflow (Peterson et al. 2002; Bamber et al. 2012; Dukhovskoy et al. 2016) are thus constrained between the shelf and open-ocean regions by these currents, potentially impacting the sensitivity of Labrador Sea deep convection to climate change (Marsh et al. 2010; Weijer et al. 2012) with consequences for the strength of the Atlantic meridional overturning circulation (Stouffer et al. 2006; Rahmstorf et al. 2015). While the governing dynamics of these Northern Hemisphere boundary currents and the ASC and ASF are more than likely to be different in nature, their effects on freshwater exchange and deep ocean convection would appear to be similar.

c. Conditions for reoccurrence of the Weddell Sea polynya in the future

In 2016 and 2017, a large polynya opened at the Maud Rise. Although this event did not develop into a fully formed open-ocean Weddell Sea polynya, it was the largest event observed since 1980 (Cheon and Gordon 2019). The opening of the Maud Rise polynyas of 2016 and 2017 has been attributed to polar cyclones (Campbell et al. 2019; Francis et al. 2019), which are expected to intensify and to shift southward into the future (Chang et al. 2012). Autonomous profiling float observations of these recent events have also revealed that intense heat loss drove deep overturning and wind-driven upwelling weakened haline stratification in the upper ocean (Campbell et al. 2019). Combined, these changes in intensity and position of winds and polar cyclones may encourage the formation of Maud Rise polynyas that could in turn evolve into full Weddell Sea polynyas.

Furthermore, the observed positive trend in the southern annular mode (Thompson et al. 2000; Thompson and Solomon 2002; Gillett and Thompson 2003; Marshall 2003; Marshall et al. 2004) is projected to continue in the future as greenhouse gas concentrations keep rising (Thompson et al. 2011). Positive phases of the southern annular mode correspond to a strengthening and a poleward shift of the Southern Hemisphere westerlies (Kushner et al. 2001; Fyfe et al. 2007; Thompson et al. 2011) which increase negative wind stress curl and the Weddell Sea Gyre within the Weddell Sea, activating mesoscale Weddell Deep Water eddies in the vicinity of Maud Rise and potentially promoting polynya events (Cheon and Gordon 2019). In contrast to this dynamic effect, the positive trend in the southern annular mode, which correlates inversely with salinity in the Weddell Sea, is thought to have resulted in fresh surface waters that could have hindered the transition of the Maud Rise polynyas to a full Weddell Sea polynya in 2017 (Cheon and Gordon 2019), and can potentially continue to impede Weddell Sea polynya formation into the future.

As more heat is brought poleward by the Weddell Sea Gyre, fed by the warming Antarctic Circumpolar Current (Gille 2002) and by the poleward heat transport by mesoscale eddies (e.g., Screen et al. 2009), and as stratification is enhanced (even moderately; see previous section), the subsurface heat reservoir may build up for a longer time (see Figs. 3 and 4). So, should convection be initiated, it could last longer or be more vigorous. This hypothesis is supported by CM2.6, which simulates a polynya as doubling of the atmospheric CO_2 is reached in the 1pctCO2 simulation that is marginally longer and larger than the polynya developing at the end of the piControl simulation, which we posit is due to the increase in the subsurface heat reservoir under climate change (Fig. 3). The buildup of the subsurface heat reservoir is also very clear in the CMIP5 models (Figs. 4b–f). This buildup has been suggested by the regional warming of the Weddell Deep Water quantified at $0.034°C\,decade^{-1}$ from 1977 to 2001 along sections of the Weddell Sea (Gille 2002; Smedsrud 2005), likely due to the warming ACC feeding the Weddell Gyre (Orsi et al. 1999), which resulted in the subsequent enhanced convergence of heat. Hence, the intensity and duration of future convection events may be more intense and over longer duration than that of the 1970s Weddell Sea polynya.

A major caveat in our results based on CMIP5 and CM2.6 models is the lack of active ice sheet components that simulate the sources of freshwater from the coast (ice sheet melting and iceberg calving) that are potential contributors to the observed freshening (Jacobs et al. 2002; Flato et al. 2013; Bronselaer et al. 2018; Moorman et al. 2020). Hence, freshening is likely underestimated in CMIP5 and CM2.6 models, which, if resolved, could lead to additional freshwater reaching the open ocean with consequences on convection. Using the GFDL-ESM2M model, Bronselaer et al. (2018) show that adding meltwater representative of ice sheet melt to the surface ocean within 3° of the coast increases the formation of Antarctic sea ice and warms the subsurface ocean around the Antarctic coast. It is thus expected that the stratification around Antarctica would be significantly affected by the addition of an active ice sheet component in CMIP5 and CM2.6 models. However, our results show that an improved representation of shelf ocean circulation in coarse-resolution climate models, akin to CM2.6, would substantially limit the propagation of this additional meltwater from the coastal region, thus constraining the associated effects to the Antarctic coasts.

In sum, future occurrence of the Weddell Sea polynya can be conceptualized as a competition between the stabilizing effect of relatively fresh surface waters, driven by surface freshening and thermodynamic effects associated with positive southern annular mode phases, and the destabilizing effect of convection triggers, such as the frequency of polar cyclones, Weddell Sea gyre strength, and meridional heat transport. In the future, if polynya triggers are not stronger or more frequent and a substantial increase in open-ocean stratification is able to occur, a slowdown or cessation of open-ocean polynya in the Weddell Sea may well be expected. If triggers become stronger and more frequent with limited open-ocean freshening, which is suggested by our analysis of CM2.6 and the expected strengthening of polynya triggers, reoccurrence of Weddell Sea polynyas may otherwise be expected.

8. Conclusions

In this study, we investigated the occurrence of the Weddell Sea polynya under climate change by comparing a large subset of the coarse-resolution CMIP5 models with the high-resolution CM2.6 climate model. Our key findings are as follows.

- Under climate change, CM2.6 forms Weddell Sea polynyas with similar timing and duration as under preindustrial forcing, whereas CMIP5 models show either a cessation or slowdown of these events under climate change.
- The cessation of convection in CMIP5 models is likely due to open-ocean surface freshening. In models, surface freshening is driven by enhanced precipitation over evaporation and sea ice north of 60°S, and by enhanced runoff from the Antarctic continent as well as changes in sea ice melting/ freezing south of 60°S.
- The circumpolar Antarctic Slope Current and associated Antarctic Slope Front are poorly resolved by the coarse-resolution CMIP5 models, whereas they are more realistically represented in CM2.6. This improved representation of shelf circulation in CM2.6 confines the coastal freshening to the shelf. As a result, CMIP5 models are more prone to large scale open-ocean freshening, leading to a slowdown, or even cessation, of Weddell Sea polynya events, whereas CM2.6 is not.

Hence, our results suggest a continuation of the open-ocean convection events and associated polynyas in the future. To allow for more accurate projections of these important climate events, an improved representation of shelf ocean circulation in climate models is needed.

REFERENCES

Baines, P. G., 2008: Mixing in downslope flows in the ocean plumes versus gravity currents. *Atmos.–Ocean*, **46**, 405–419, https:// doi.org/10.3137/ao.460402.

Bamber, J., M. van den Broeke, J. Ettema, J. Lenaerts, and E. Rignot, 2012: Recent large increases in freshwater fluxes from Greenland into the North Atlantic. *Geophys. Res. Lett.*, **39**, L19501, https://doi.org/10.1029/2012GL052552.

Beadling, R. L., J. L. Russell, R. J. Stouffer, P. J. Goodman, and M. Mazloff, 2019: Assessing the quality of Southern Ocean circulation in CMIP5 AOGCM and Earth system model simulations. *J. Climate*, **32**, 5915–5940, https://doi.org/10.1175/JCLI-D-19-0263.1.

Beckmann, A., and A. F. Pereira, 2003: Lateral tidal mixing in the Antarctic marginal seas. *Ocean Dyn.*, **53**, 21–26, https:// doi.org/10.1007/s10236-002-0020-9.

Boyer, T., and Coauthors, 2018: World Ocean Database 2018. NOAA Atlas NESDIS 87, 207 pp., https://data.nodc.noaa.gov/woa/WOD/DOC/wod_intro.pdf.

Bracegirdle, T. J., E. Shuckburgh, J. Sallee, Z. Wang, A. J. S. Meijers, N. Bruneau, T. Phillips, and L. J. Wilcox, 2013: Assessment of surface winds over the Atlantic, Indian, and Pacific Ocean sectors of the Southern Ocean in CMIP5 models: Historical bias, forcing response, and state dependence. *J. Geophys. Res. Atmos.*, **118**, 547–562, https://doi.org/10.1002/jgrd.50153.

Bronselaer, B., M. Winton, S. Griffies, W. Hurlin, K. Rodgers, O. Sergienko, R. Stouffer, and J. Russell, 2018: Change in future climate due to Antarctic meltwater. *Nature*, **564**, 53–58, https://doi.org/10.1038/s41586-018-0712-z.

Campbell, E., E. Wilson, G. Moore, S. Riser, C. Brayton, M. Mazloff, and L. Talley, 2019: Antarctic offshore polynyas linked to Southern Hemisphere climate anomalies. *Nature*, **570**, 319, https://doi.org/10.1038/s41586-019-1294-0.

Carsey, F. D., 1980: Microwave observation of the Weddell Polynya. *Mon. Wea. Rev.*, **108**, 2032–2044, https://doi.org/10.1175/1520-0493(1980)108<2032:MOOTWP>2.0.CO;2.

Chang, E. K. M., Y. Guo, and X. Xia, 2012: CMIP5 multimodel ensemble projection of storm track change under global warming. *J. Geophys. Res.*, **117**, D23118, https://doi.org/10.1029/2012JD018578.

Cheon, W. G., and A. Gordon, 2019: Open-ocean polynyas and deep convection in the Southern Ocean. *Sci. Rep.*, **9**, 6935, https://doi.org/10.1038/s41598-019-43466-2.

——, Y.-G. Park, J. R. Toggweiler, and S.-K. Lee, 2014: The relationship of Weddell Polynya and open-ocean deep convection to the Southern Hemisphere westerlies. *J. Phys. Oceanogr.*, **44**, 694–713, https://doi.org/10.1175/JPO-D-13-0112.1.

Comiso, J. C., and A. L. Gordon, 1987: Recurring polynyas over the Cosmonaut Sea and the Maud Rise. *J. Geophys. Res.*, **92**, 2819–2833, https://doi.org/10.1029/JC092iC03p02819.

de Boyer Montégut, C., G. Madec, A. S. Fischer, A. Lazar, and D. Iudicone, 2004: Mixed layer depth over the global ocean: An examination of profile data and a profile-based climatology. *J. Geophys. Res.*, **109**, C12003, https://doi.org/10.1029/2004JC002378.

Dee, D. P., and Coauthors, 2011: The ERA-Interim reanalysis: Configuration and performance of the data assimilation system. *Quart. J. Roy. Meteor. Soc.*, **137**, 553–597, https://doi.org/10.1002/qj.828.

de Lavergne, C., J. B. Palter, E. D. Galbraith, R. Bernardello, and I. Marinov, 2014: Cessation of deep convection in the open Southern Ocean under anthropogenic climate change. *Nat. Climate Change*, **4**, 278–282, https://doi.org/10.1038/nclimate2132.

Delworth, T. L., and Coauthors, 2012: Simulated climate and climate change in the GFDL CM2.5 high-resolution coupled climate model. *J. Climate*, **25**, 2755–2781, https://doi.org/10.1175/JCLI-D-11-00316.1.

Dufour, C. O., A. K. Morrison, S. M. Griffies, I. Frenger, H. Zanowski, and M. Winton, 2017: Preconditioning of the Weddell Sea Polynya by the ocean mesoscale and dense water overflows. *J. Climate*, **30**, 7719–7737, https://doi.org/10.1175/JCLI-D-16-0586.1.

Dukhovskoy, D. S., and Coauthors, 2016: Greenland freshwater pathways in the sub-Arctic seas from model experiments with passive tracers. *J. Geophys. Res. Oceans*, **121**, 877–907, https://doi.org/10.1002/2015JC011290.

ECMWF, 2011: ECMWF's Operational Model Analysis, starting in 2011. Research Data Archive at the National Center for Atmospheric Research, Computational and Information Systems Laboratory, accessed 2020, https://doi.org/10.5065/D6ZG6Q9F.

Enderlin, E. M., I. M. Howat, S. Jeong, M.-J. Noh, J. H. van Angelen, and M. R. van den Broeke, 2014: An improved mass budget for the Greenland ice sheet. *Geophys. Res. Lett.*, **41**, 866–872, https://doi.org/10.1002/2013GL059010.

Flato, G., and Coauthors, 2013: Evaluation of climate models. *Climate Change 2013: The Physical Science Basis*, T. F. Stocker et al., Eds., Cambridge University Press, 741–866.

Fox-Kemper, B., and Coauthors, 2011: Parameterization of mixed layer eddies. III: Implementation and impact in global ocean climate simulations. *Ocean Modell.*, **39**, 61–78, https://doi.org/10.1016/j.ocemod.2010.09.002.

Francis, D., C. Eayrs, J. Cuesta, and D. Holland, 2019: Polar cyclones at the origin of the reoccurrence of the Maud Rise polynya in austral winter 2017. *J. Geophys. Res. Atmos.*, **124**, 5251–5267, https://doi.org/10.1029/2019JD030618.

Fyfe, J. C., O. A. Saenko, K. Zickfeld, M. Eby, and A. J. Weaver, 2007: The role of poleward-intensifying winds on Southern Ocean warming. *J. Climate*, **20**, 5391–5400, https://doi.org/10.1175/2007JCLI1764.1.

Gille, S. T., 2002: Warming of the Southern Ocean since the 1950s. *Science*, **295**, 1275–1277, https://doi.org/10.1126/science.1065863.

Gillett, N. P., and D. W. J. Thompson, 2003: Simulation of recent Southern Hemisphere climate change. *Science*, **302**, 273–275, https://doi.org/10.1126/science.1087440.

Goddard, P. B., C. O. Dufour, J. Yin, S. M. Griffies, and M. Winton, 2017: CO_2-induced ocean warming of the Antarctic continental shelf in an eddying global climate model. *J. Geophys. Res. Oceans*, **122**, 8079–8101, https://doi.org/10.1002/2017JC012849.

Gordon, A. L., 1978: Deep Antarctic convection west of Maud Rise. *J. Phys. Oceanogr.*, **8**, 600–612, https://doi.org/10.1175/1520-0485(1978)008<0600:DACWOM>2.0.CO;2.

——, 1982: Weddell Deep Water variability. *J. Mar. Res.*, **40**, 199–217.

——, M. Visbeck, and J. C. Comiso, 2007: A possible link between the Weddell Polynya and the southern annular mode. *J. Climate*, **20**, 2558–2571, https://doi.org/10.1175/JCLI4046.1.

Gouretski, V., 2018: WOCE-ARGO global hydrographic climatology. *Ocean Sci. Discuss.*, https://doi.org/10.5194/os-2018-34.

Griffies, S. M., and Coauthors, 2015: Impacts on ocean heat from transient mesoscale eddies in a hierarchy of climate models. *J. Climate*, **28**, 952–977, https://doi.org/10.1175/JCLI-D-14-00353.1.

Hallberg, R., 2013: Using a resolution function to regulate parameterizations of oceanic mesoscale eddy effects. *Ocean Modell.*, **72**, 92–103, https://doi.org/10.1016/j.ocemod.2013.08.007.

Haumann, F. A., N. Gruber, M. Münnich, I. Frenger, and S. Kern, 2016: Antarctic sea-ice freshwater fluxes associated with freezing, transport, and melting. ETH Zurich, https://doi.org/10.16904/8.

Heuzé, C., K. J. Heywood, D. P. Stevens, and J. K. Ridley, 2013: Southern Ocean bottom water characteristics in CMIP5 models. *Geophys. Res. Lett.*, **40**, 1409–1414, https://doi.org/10.1002/grl.50287.

——, ——, ——, and ——, 2015: Changes in global ocean bottom properties and volume transports in CMIP5 models under climate change scenarios. *J. Climate*, **28**, 2917–2944, https://doi.org/10.1175/JCLI-D-14-00381.1.

Heywood, K. J., and Coauthors, 2014: Ocean processes at the Antarctic continental slope. *Philos. Trans. Roy. Soc.*, **372A**, 20130047, https://doi.org/10.1098/rsta.2013.0047.

Holland, D. M., 2001: Explaining the Weddell polynya—A large ocean eddy shed at Maud Rise. *Science*, **292**, 1697–1700, https://doi.org/10.1126/science.1059322.

Jacobs, S. S., 1991: On the nature and significance of the Antarctic Slope Front. *Mar. Chem.*, **35**, 9–24, https://doi.org/10.1016/S0304-4203(09)90005-6.

——, C. F. Giulivi, and P. A. Mele, 2002: Freshening of the Ross Sea during the late 20th century. *Science*, **297**, 386–389, https://doi.org/10.1126/science.1069574.

Jena, B., M. Ravichandran, and J. Turner, 2019: Recent re-occurrence of large open-ocean polynya on the Maud Rise seamount. *Geophys. Res. Lett.*, **46**, 4320–4329, https://doi.org/10.1029/2018GL081482.

Klinger, B. A., J. Marshall, and U. Send, 1996: Representation of convective plumes by vertical adjustment. *J. Geophys. Res.*, **101**, 18 175–18 182, https://doi.org/10.1029/96JC00861.

Kurtakoti, P., M. Veneziani, A. Stössel, and W. Weijer, 2018: Preconditioning and formation of Maud Rise polynyas in a high-resolution Earth system model. *J. Climate*, **31**, 9659–9678, https://doi.org/10.1175/JCLI-D-18-0392.1.

Kushner, P. J., I. M. Held, and T. L. Delworth, 2001: Southern Hemisphere atmospheric circulation response to global warming. *J. Climate*, **14**, 2238–2249, https://doi.org/10.1175/1520-0442(2001)014<0001:SHACRT>2.0.CO;2.

Large, W. G., J. C. McWilliams, and S. C. Doney, 1994: Oceanic vertical mixing: A review and a model with a nonlocal boundary layer parameterization. *Rev. Geophys.*, **32**, 363–403, https://doi.org/10.1029/94RG01872.

Lazier, J. R. N., and D. G. Wright, 1993: Annual velocity variations in the Labrador Current. *J. Phys. Oceanogr.*, **23**, 659–678, https://doi.org/10.1175/1520-0485(1993)023<0659:AVVITL>2.0.CO;2.

Marsh, R., D. Desbruyères, J. L. Bamber, B. A. de Cuevas, A. C. Coward, and Y. Aksenov, 2010: Short-term impacts of en-hanced Greenland freshwater fluxes in an eddy-permitting ocean model. *Ocean Sci.*, **6**, 749–760, https://doi.org/10.5194/os-6-749-2010.

Marshall, G. J., 2003: Trends in the southern annular mode from observations and reanalyses. *J. Climate*, **16**, 4134–4143, https://doi.org/10.1175/1520-0442(2003)016<4134:TITSAM>2.0.CO;2.

——, P. A. Stott, J. Turner, W. M. Connolley, J. C. King, and T. A. Lachlan-Cope, 2004: Causes of exceptional atmospheric cir-culation changes in the Southern Hemisphere. *Geophys. Res. Lett.*, **31**, L14205, https://doi.org/10.1029/2004GL019952.

Martin, T., W. Park, and M. Latif, 2013: Multi-centennial vari-ability controlled by Southern Ocean convection in the Kiel Climate Model. *Climate Dyn.*, **40**, 2005–2022, https://doi.org/10.1007/s00382-012-1586-7.

Martinson, D. G., P. D. Killworth, and A. L. Gordon, 1981: A convective model for the Weddell polynya. *J. Phys. Oceanogr.*, **11**, 466–488, https://doi.org/10.1175/1520-0485(1981)011<0466:ACMFTW>2.0.CO;2.

Meijers, A. J. S., 2014: The Southern Ocean in the Coupled Model Intercomparison Project phase. *Philos. Trans. Roy. Soc.*, **372A**, 20130296, https://doi.org/10.1098/rsta.2013.0296.

Moore, G., K. Alverson, and I. Renfrew, 2002: A reconstruction of the air–sea interaction associated with the Weddell polynya. *J. Phys. Oceanogr.*, **32**, 1685–1698, https://doi.org/10.1175/1520-0485(2002)032<1685:AROTAS>2.0.CO;2.

Moorman, R., A. K. Morrison, and A. M. Hogg, 2020: Thermal responses to Antarctic ice shelf melt in an eddy-rich global ocean–sea ice model. *J. Climate*, **33**, 6599–6620, https://doi.org/10.1175/JCLI-D-19-0846.1.

Murray, R. J., 1996: Explicit generation of orthogonal grids for ocean models. *J. Comput. Phys.*, **126**, 251–273, https://doi.org/10.1006/jcph.1996.0136.

Orsi, A., G. Johnson, and J. Bullister, 1999: Circulation, mixing, and production of Antarctic bottom water. *Prog. Oceanogr.*, **43**, 55–109, https://doi.org/10.1016/S0079-6611(99)00004-X.

Peterson, B. J., R. M. Holmes, J. W. McClelland, C. J. Vörösmarty, R. B. Lammers, A. I. Shiklomanov, I. A. Shiklomanov, and S. Rahmstorf, 2002: Increasing river discharge to the Arctic Ocean. *Science*, **298**, 2171–2173, https://doi.org/10.1126/science.1077445.

Rahmstorf, S., J. Box, G. Feulner, M. Mann, A. Robinson, S. Rutherford, and E. Schaffernicht, 2015: Exceptional twentieth-century slowdown in Atlantic Ocean overturning circulation. *Nat. Climate Change*, **5**, 475–480, https://doi.org/10.1038/nclimate2554.

Rayner, N. A., D. E. Parker, E. B. Horton, C. K. Folland, L. V. Alexander, D. P. Rowell, E. C. Kent, and A. Kaplan, 2003: Global analyses of sea surface temperature, sea ice, and night marine air temperature since the late nineteenth century. *J. Geophys. Res.*, **108**, 4407, https://doi.org/10.1029/2002JD002670.

Reintges, A., T. Martin, M. Latif, and W. Park, 2017: Physical controls of Southern Ocean deep-convection variability in CMIP5 models and the Kiel climate model. *Geophys. Res. Lett.*, **44**, 6951–6958, https://doi.org/10.1002/2017GL074087.

Rocha, C. B., T. K. Chereskin, S. T. Gille, and D. Menemenlis, 2016: Mesoscale to submesoscale wavenumber spectra in Drake Passage. *J. Phys. Oceanogr.*, **46**, 601–620, https://doi.org/10.1175/JPO-D-15-0087.1.

Screen, J. A., N. P. Gillett, D. P. Stevens, G. J. Marshall, and H. K. Roscoe, 2009: The role of eddies in the Southern Ocean tem-perature response to the southern annular mode. *J. Climate*, **22**, 806–818, https://doi.org/10.1175/2008JCLI2416.1.

Sloyan, B. M., and I. V. Kamenkovich, 2007: Simulation of Subantarctic Mode and Antarctic Intermediate Waters in climate models. *J. Climate*, **20**, 5061–5080, https://doi.org/10.1175/JCLI4295.1.

Smedsrud, L., 2005: Warming of the deep water in the Weddell Sea along the Greenwich meridian: 1977–2001. *Deep-Sea Res. I*, **52**, 241–258, https://doi.org/10.1016/j.dsr.2004.10.004.

Stewart, A. L., and A. F. Thompson, 2015: Eddy-mediated trans-port of warm Circumpolar Deep Water across the Antarctic Shelf Break. *Geophys. Res. Lett.*, **42**, 432–440, https://doi.org/10.1002/2014GL062281.

——, A. Klocker, and D. Menemenlis, 2018: Circum-Antarctic shoreward heat transport derived from an eddy- and tide-resolving simulation. *Geophys. Res. Lett.*, **45**, 834–845, https://doi.org/10.1002/2017GL075677.

——, ——, and ——, 2019: Acceleration and overturning of the Antarctic Slope Current by winds, eddies, and tides. *J. Phys. Oceanogr.*, **49**, 2043–2074, https://doi.org/10.1175/JPO-D-18-0221.1.

St-Laurent, P., J. M. Klinck, and M. S. Dinniman, 2013: On the role of coastal troughs in the circulation of warm Circumpolar Deep Water on Antarctic shelves. *J. Phys. Oceanogr.*, **43**, 51–64, https://doi.org/10.1175/JPO-D-11-0237.1.

Stössel, A., D. Notz, F. A. Haumann, H. Haak, J. Jungclaus, and U. Mikolajewicz, 2015: Controlling high-latitude Southern Ocean convection in climate models. *Ocean Modell.*, **86**, 58–75, https://doi.org/10.1016/j.ocemod.2014.11.008.

Stouffer, R. J., and Coauthors, 2006: Investigating the causes of the response of the thermohaline circulation to past and future climate changes. *J. Climate*, **19**, 1365–1387, https://doi.org/10.1175/JCLI3689.1.

Swart, N. C., and J. C. Fyfe, 2012: Observed and simulated changes in the Southern Hemisphere surface westerly wind-stress. *Geophys. Res. Lett.*, **39**, L16711, https://doi.org/10.1029/2012GL052810.

Taylor, K. E., R. J. Stouffer, and G. A. Meehl, 2012: An overview of CMIP5 and the experiment design. *Bull. Amer. Meteor. Soc.*, **93**, 485–498, https://doi.org/10.1175/BAMS-D-11-00094.1.

Thompson, A., A. Stewart, P. Spence, and K. Heywood, 2018: The Antarctic Slope Current in a changing climate. *Rev. Geophys.*, **56**, 741–770, https://doi.org/10.1029/2018RG000624.

Thompson, D. W. J., and S. Solomon, 2002: Interpretation of recent Southern Hemisphere climate change. *Science*, **296**, 895–899, https://doi.org/10.1126/science.1069270.

——, J. M. Wallace, and G. C. Hegerl, 2000: Annular modes in the extratropical circulation. Part II: Trends. *J. Climate*, **13**, 1018–1036, https://doi.org/10.1175/1520-0442(2000)013<1018:AMITEC>2.0.CO;2.

——, S. Solomon, P. Kushner, M. England, K. Grise, and D. Karoly, 2011: Signatures of the Antarctic ozone hole in Southern Hemisphere surface climate change. *Nat. Geosci.*, **4**, 741–749, https://doi.org/10.1038/ngeo1296.

Weijer, W., M. E. Maltrud, M. W. Hecht, H. A. Dijkstra, and M. A. Kliphuis, 2012: Response of the Atlantic Ocean circulation to Greenland Ice Sheet melting in a strongly-eddying ocean model. *Geophys. Res. Lett.*, **39**, L09606, https://doi.org/10.1029/2012GL051611.

Whitworth, T., A. H. Orsi, S.-J. Kim, W. D. Nowlin Jr., and R. A. Locarnini, 2013: Water masses and mixing near the Antarctic slope front. *Ocean, Ice, and Atmosphere: Interactions at the Antarctic Continental Margin*, *Geophys. Monogr.*, Vol. 75, Amer. Geophys. Union, 1–27.

Winton, M., 2000: A reformulated three-layer sea ice model. *J. Atmos. Oceanic Technol.*, **17**, 525–531, https://doi.org/10.1175/1520-0426(2000)017<0525:ARTLSI>2.0.CO;2.

——, R. Hallberg, and A. Gnanadesikan, 1998: Simulation of density-driven frictional downslope flow in *z*-coordinate ocean models. *J. Phys. Oceanogr.*, **28**, 2163–2174, https://doi.org/10.1175/1520-0485(1998)028<2163:SODDFD>2.0.CO;2.

——, W. G. Anderson, T. L. Delworth, S. M. Griffies, W. J. Hurlin, and A. Rosati, 2014: Has coarse ocean resolution biased simulations of transient climate sensitivity? *Geophys. Res. Lett.*, **41**, 8522–8529, https://doi.org/10.1002/2014GL061523.